

# **Investigating How the Choice of Stratospheric Meteorological Data Influences Volcanic Ash Forecasts Within the London VAAC Area of Responsibility**

Technical Report No. 647

September 2021

Nicola Stebbing, Frances Beckett and Andrew Jones

## Contents

Contents .....	2
Abstract.....	3
1. Introduction.....	4
1.1. The Importance of Forecasting the Movement of Volcanic Ash.....	4
1.2. The London VAAC Operational Procedure .....	4
1.3. Plume Height Frequencies.....	5
1.4. Previous Investigations Using Higher Altitude Meteorological Data.....	5
1.5. Aims for This Study.....	6
2. Case Study Overview.....	8
2.1. Stratospheric Warming Events.....	9
2.2. Vortex Recovery and Intensification Events .....	11
2.3. Summer .....	11
3. Methods.....	12
3.1. Meteorological Data Acquisition and Setup.....	12
3.2. NAME Setup and Outputs.....	13
3.3. Statistical Analysis .....	13
4. Analysis .....	15
4.1. Sensitivity to Plume Height .....	15
4.2. Sensitivity to Stratospheric Conditions .....	17
4.2.1. Stratospheric Warming Events.....	17
4.2.2. Vortex Recovery and Intensification Events .....	20
4.2.3. Summer .....	23
5. Discussion .....	27
5.1. Overarching Observations from the Case Studies.....	27
5.2. Limitations of this Study .....	28
5.3. Technical Considerations.....	29
6. Conclusions .....	31
7. Acknowledgements.....	32
References .....	33
Appendix.....	37

## Abstract

Volcanic ash presents multiple hazards to aircraft, from reduced pilot visibility to permanent engine damage. To mitigate the risk of an aircraft encountering an ash cloud, Volcanic Ash Advisory Centres (VAACs) provide forecasts on the expected location of volcanic ash in the atmosphere. The London VAAC uses the atmospheric dispersion model NAME (Numerical Atmospheric-dispersion Modelling Environment), driven by meteorological parameters from the Met Office Unified Model (MetUM), to generate forecasts within its area of responsibility. However, due to historical computational restraints, the dispersion model domain is currently restricted to altitudes < 30 km, despite MetUM data being available up to an altitude of 80 km. The likelihood of an eruption releasing ash at altitudes > 30 km is non-zero and thus the decision has been made to remove this height restriction.

Here, we explore two options to introduce the capability to model volcanic ash dispersion above 30 km at the London VAAC. The first option uses a 'persisted' meteorology approach above 30 km, while the second option uses the full meteorological forecast conditions. The first option assumes that upper stratospheric meteorological conditions above 30 km are similar enough to the conditions forecast at 30 km that any differences are negligible. To investigate the appropriateness of this assumption, we considered a hypothetical eruption of Öraefajökull (Iceland) during different stratospheric meteorological scenarios, including Sudden Stratospheric Warming (SSW), Vortex Intensification (VI) and Final Stratospheric Warming (FSW) events.

We found that, when ash is released up to 35 km, using persisted meteorological conditions underestimates the horizontal spread of upper-level ash perpendicular to the main dispersal path of the ash cloud in every scenario. During events when there was a significant shift in stratospheric zonal wind direction or speed, such as SSWs, VIs and FSWs, we found that the ash dispersed by the persisted meteorology reacted to the changes in wind conditions later than that dispersed using the full forecast data, leading to differences in both the distance and direction the simulated ash clouds were dispersed. When stratospheric conditions were less variable, such as during summer periods, fewer differences in the spread of the simulated ash clouds were found, but large differences in the ash concentrations and mass loadings in the centre of the ash clouds were observed. Additionally, when simulations using a limited depth release, to mimic umbrella clouds, were compared, the differences between the modelled ash clouds were further exaggerated. These results suggest that stratospheric conditions above 30 km can have a significant impact on the forecast atmospheric location and concentration of volcanic ash released near to and above 30 km, and in order to best represent the dispersion of ash above 30 km in operational volcanic ash forecasting all available MetUM data covering the altitudes volcanic ash is likely to reach should be used.

## 1. Introduction

### 1.1. The Importance of Forecasting the Movement of Volcanic Ash

In the event of a volcanic eruption generating an ash cloud, there are nine Volcanic Ash Advisory Centres (VAACs) in place around the world to forecast their movement to warn aircraft pilots (Leadbetter and Hort 2011, Newhall et al. 2018). Ash clouds present a hazard to aircraft both due to the impact on visibility for the pilot and the effects on the plane itself. In the air, aircraft encounters with volcanic ash can lead to surface abrasion, temporary engine failure and, in some cases, permanent engine damage (Casadevall 1994). On the ground, ash can be ingested into aircraft engines during taxiing, take-off and landing and affect the manoeuvrability of the aircraft (Casadevall et al. 1996). Although, to date, no crashes or fatalities have resulted from encounters with volcanic ash, the cost of repairing a damaged aircraft alone is estimated to be of the order of several million (US) dollars, not accounting for the cost of taking the plane out of service temporarily (Newhall et al. 2018). The forced halting of the aviation industry can have major economic impacts as well, with the 2010 eruption of Eyjafjallajökull, Iceland leading to global GDP losses of US\$5.0 billion (Oxford Economics 2010). Therefore, it is important for the aviation sector to receive accurate information on the location and concentration of volcanic ash in the atmosphere.

### 1.2. The London VAAC Operational Procedure

The London VAAC is tasked with forecasting the movement and dispersion of volcanic ash clouds within the north-eastern corner of the North Atlantic, which includes any produced by eruptions in Iceland and Jan Mayen (Norway). This forecasting capability is achieved using the atmospheric dispersion model NAME (Numerical Atmospheric-dispersion Modelling Environment, Jones et al. 2007). Operationally, NAME is driven by meteorological parameters from the global configuration of the Met Office Unified Model (MetUM), with a temporal resolution of 3 hours, a horizontal resolution of approximately 10 km and using 59 vertical levels between the surface and 30 km asl (Beckett et al. 2020, Witham et al. 2020). Although the MetUM produces data over 70 vertical levels (up to 80 km asl), only 59 levels are used with NAME for the London VAAC in order to decrease run times during an event and lessen data storage requirements. However, as a result, the maximum plume height which can be modelled is limited to 30 km. This is further reduced to approximately 25 km if the buoyant plume model is used to estimate the plume height, due to its bisection method that finds solutions for plume heights greater than and smaller than the initial height given (Devenish 2013). If an eruption larger than 30 km were to occur in Iceland with the current set-up in place, the model ash particles released above 30 km would immediately be removed due to a lack of valid meteorological (met) conditions. This in turn would lead to reduced total column ash mass loadings (Figure 1a) and reduced horizontal spread due to the missing upper-level ash (Figure 1b). Additionally, if the London VAAC were called in to assist with an eruption producing ash above 30 km elsewhere in the world, for example in the tropics where plume heights can be larger due to the effects of the unstable, moist atmosphere (Tupper et al. 2009), the same problems would occur.

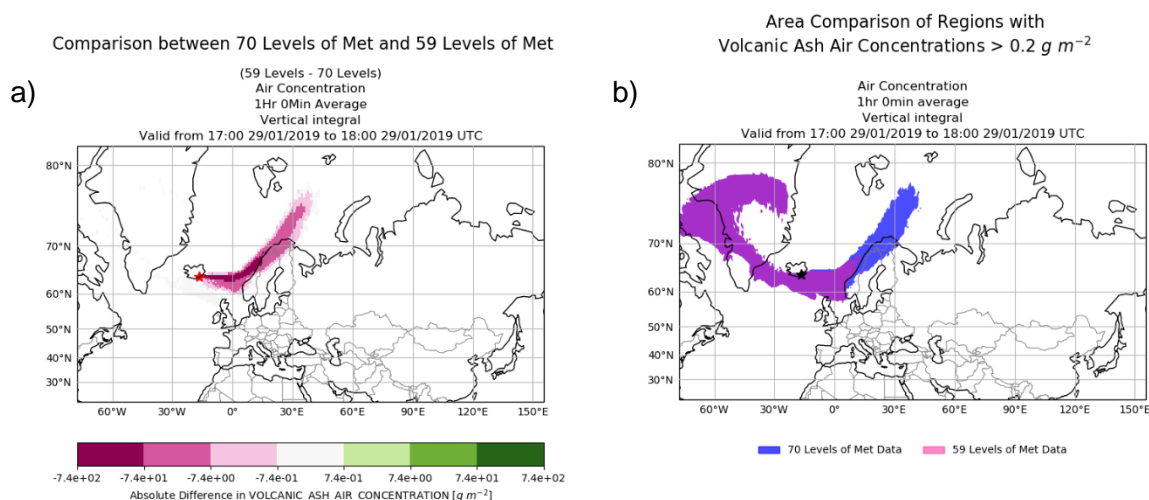


Figure 1: Example of the error in the forecast plume dispersal if an eruption producing a plume  $> 30 \text{ km}$  occurred with the current VAAC set-up. Comparison of simulated ash clouds produced using 59 levels of met data and 70 levels of met data for a simulated  $35 \text{ km}$  eruption on 28/01/2019 after  $T+36$ . a) The difference in simulated ash mass loading values. b) The horizontal spread of ash cloud areas with ash mass loadings  $> 0.2 \text{ g m}^{-2}$ ; the purple region represents an ash cloud area forecast by both met scenarios.

### 1.3. Plume Height Frequencies

The relative explosivity of a volcanic eruption is described using the Volcanic Explosivity Index (Newhall and Self 1982), with the explosivity value assigned based on the volume of erupted material, the plume height, the length of eruption and other qualitative observations. A plume height over  $25 \text{ km}$  will put an eruption at VEI 5 or above. The frequency of eruptions with plumes  $> 30 \text{ km}$  can therefore fit within the global recurrence frequency of VEI 5 to VEI 8, from 1 per decade to less than 1 per millennia (Simkin 1993, Kiyosugi et al. 2015). In Iceland, there have been three known VEI 6 events: the 1362 AD eruption of Öräfajökull, with an estimated plume height of  $25\text{--}37 \text{ km}$ , and the Hekla 3 and Hekla 4 eruptions, in circa 2800 BP and 4000 BP respectively, with suggested plume heights of  $30\text{--}35 \text{ km}$  (Lacasse 2001, Barsotti et al. 2018). Additionally, the 1875 AD Askja eruption has been estimated to have had a maximum plume height between  $25\text{--}37 \text{ km}$  (Lacasse 2001, Carey et al. 2010) and tephra fallout from past eruptions at Katla implies plume heights were between  $20\text{--}35 \text{ km}$  (Lacasse 2001, Saxby et al. 2020), putting these eruptions within the VEI 5 and up category as well.

### 1.4. Previous Investigations Using Higher Altitude Meteorological Data

Previous research which has modelled high altitude ash releases from volcanic activity in Iceland has used a variety of methods to account for upper-level atmospheric dynamics. To investigate the conditions needed for tephra to reach the historical and prehistorical deposit locations found around the subpolar North Atlantic, Lacasse (2001) used a mixture of seasonally averaged rawinsonde data from four subpolar meteorological stations for below  $25 \text{ km}$  and seasonally averaged radiosonde and satellite observations up to  $48 \text{ km}$ . Barsotti et al. (2018) used ten years of ERA-INTERIM met data, which has a  $0.7^\circ$  horizontal resolution and uses 60 vertical levels up to  $0.1 \text{ hPa}$  ( $\sim 65 \text{ km}$ ) (Berrisford et al. 2009), to assess the impact of a modern-day reoccurrence of the 1362 AD eruption of Öräfajökull on Iceland's infrastructure. Utilising the same met data and model as the London VAAC, Saxby et al. (2020) investigated

whether the transport of volcanic ash was sensitive to the use of ‘persisted’ or ‘real’ met data above 30 km. Their ‘persisted’ met data used met conditions from the 59<sup>th</sup> model level for altitudes higher than the 30 km limit, while their ‘real’ met data used all 70 available levels of MetUM data, up to 80 km. Saxby et al. (2020) conducted a sensitivity analysis using NAME runs for a release of ash from Katla over 1 hour, using a uniform particle size and uniform particle distribution from summit to plume top heights of 25 km and 35 km. They found relatively little difference in the ash distribution in the atmosphere between using the ‘persisted’ and ‘real’ met conditions in the two hours after the eruption end time. However, they only looked at a single, brief wintertime event and the results from Lacasse (2001) show that stratospheric conditions vary throughout the seasons, so it is likely that the level of similarity between the met data options will not remain the same over the course of the year. On the other hand, Barsotti et al. (2018) did take the varying met conditions into account in their simulations, but given the lack of time constraints for research simulations they did not need to consider using less than the full amount of met data available to them. Thus, we will take inspiration from the methods of Lacasse (2001) and Barsotti et al. (2018) to expand upon the investigation started by Saxby et al. (2020) and apply it to our operational context.

### **1.5. Aims for This Study**

We consider two options for using MetUM with NAME for modelling volcanic plumes above the current 30 km altitude limit, as used by Saxby et al. (2020):

1. Assume that the stratospheric met conditions above 30 km are similar enough to the conditions at 30 km that any differences are negligible and use the model met conditions at 30 km for higher altitudes, persisting the met data from the 59<sup>th</sup> vertical level (Met<sub>P</sub>).
2. Use the full forecast met conditions above the current 30 km limit, i.e. use all 70 vertical levels of met data (Met<sub>70</sub>).

Figure 2 shows an example of the differences in the Met<sub>P</sub> and Met<sub>70</sub> wind parameters above the Öraefajökull vent. In this case, the Met<sub>P</sub> winds are slower and near westerly above 30 km, while the Met<sub>70</sub> winds are faster and vary slightly in their direction. Therefore, the aims of this study are to investigate whether differences in met conditions above 30 km are significant enough under different meteorological situations over altitudes ash is likely to reach to affect the ash dispersal forecasts produced by the London VAAC and to consider the technical advantages and disadvantages to choosing either approach.

In order to adequately compare the forecast ability of the two met data options, six different case studies were chosen for analysis that encompass different stratospheric meteorological conditions over high latitudes throughout the year. For each, three plume heights with uniform releases of ash (25 km, 30 km and 35 km asl) are considered to determine whether the differences in the meteorological conditions above 30 km have a more significant impact on plume dispersal differences with increasing plume height. Large explosive eruptions can also result in the formation of an umbrella cloud, where the buoyant plume rapidly expands radially from the volcano upon reaching an altitude where the plume’s density matches that of the surrounding atmosphere (Sparks 1986, Webster et al. 2020). Thus, to represent this type of

event, we also consider a scenario where ash is released over a limited depth, between 30 and 35 km. To model these conditions, a hypothetical eruption of Öraefajökull was considered. Among the Icelandic volcanoes that have a likelihood of producing eruptive plumes taller than 30 km, Öraefajökull has shown the most recent signs of unrest, from November 2017 to May 2018 (Barsotti et al., 2018).

Model Meteorology above ORAEFAJOKULL, 18:00 29/01/2019 UTC  
And Vertical Data Levels for the UM Global Model

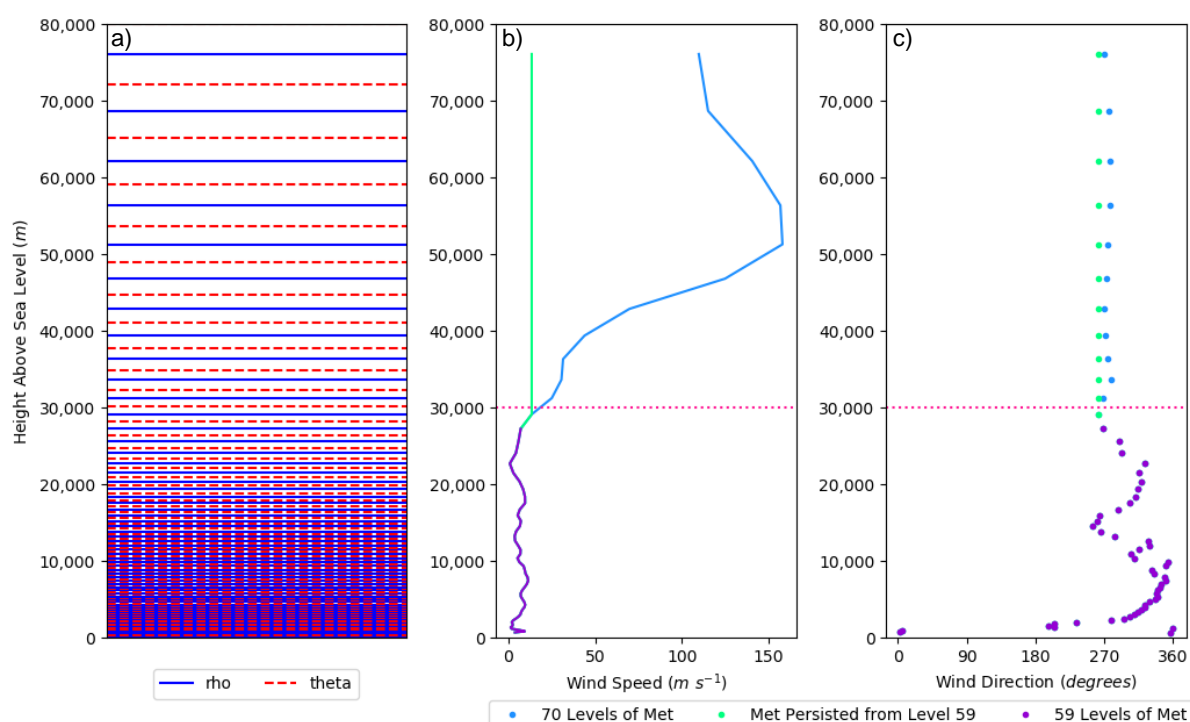


Figure 2: (a) The MetUM vertical levels from which the met data are ingested. The blue solid lines represent the 'rho' levels on which the wind vector data are stored, the red dashed lines represent the 'theta' levels on which temperature data are stored. An example of the difference in model horizontal (b) wind speed and (c) wind direction above Öraefajökull as NAME interprets them when using Met<sub>P</sub> compared to Met<sub>70</sub> are also shown. The pink dotted line shows the 30 km cut-off height.

## 2. Case Study Overview

The following background information and summaries of each case study aim to explain the meteorological phenomena they encompass and the differences in plume dispersal we might expect to see in the NAME simulations as a result.

*In winter, the **polar stratosphere** is characterised by the stratospheric polar vortex, a planetary-scale cyclonic circulation that forms over the winter pole due to the Earth's axial tilt leading to radiative cooling from a lack of solar heating. The cold air within the polar vortex can reach temperatures  $< -80\text{ }^{\circ}\text{C}$  and is accompanied by the surrounding westerly polar night jet stream (Lee and Butler 2020). These westerly winds increase in speed with altitude and are stronger in the southern hemisphere (Craig 1965) where the winter vortex is more stable due to the presence of the Southern Ocean surrounding Antarctica (Lee and Butler 2020). During the summer, while lower stratospheric winds, from the tropopause to around 15 to 20 km, remain westerly in polar regions, in the upper stratosphere, winds are easterly (Hare 1960, Craig 1965, Lacasse 2001). The winds become more easterly with height and latitude and intensify as summer progresses, lasting May through August (Hare 1960). The strength of the upper-level Arctic easterly winds is smaller than the equivalent westerlies in winter, however, with magnitudes at  $\sim 48\text{ km}$  (1 hPa) of less than  $12\text{ m s}^{-1}$  in April-May and August and up to  $25\text{ m s}^{-1}$  in June and July in comparison to values of  $40\text{--}45\text{ m s}^{-1}$  in autumn and winter (Lacasse 2001).*

**Sudden stratospheric warming** events (SSWs) are the result of tropospheric planetary-scale waves propagating vertically into the westerly winds of the wintertime stratospheric polar vortex. The waves break in the stratosphere, depositing their momentum and decelerating the westerly flow. Accompanying this deceleration in wind strength is a dramatic warming of the polar stratosphere by as much as  $30\text{--}40\text{ K}$  in a few days, along with the displacement and/or split of the stratospheric polar vortex. In major SSW events, the zonal-mean zonal winds are decelerated to the extent that they reverse completely to become easterly (Butler et al. 2017, Lee and Butler 2020). In the Northern Hemisphere, this reversal is defined when the daily-mean zonal-mean zonal wind at 10 hPa (approximately 30 km) and  $60^{\circ}\text{N}$  ( $U_{10,60}$ ) first changes from westerly to easterly, with such major events occurring on average six times per decade (Charlton and Polvani 2007, Lee and Butler 2020). The wind and temperature anomalies descend from the upper to lower stratosphere (Limpasuvan et al. 2004) as subsequent planetary-scale waves break lower down in the atmosphere because they can only propagate into regions of westerly flow (Lee and Butler 2020) and upper-level winds are now easterly. Vortex recovery after an SSW occurs through radiative cooling in the mid-to-upper stratosphere as the lower-level easterlies 'shield' the upper levels from further planetary-scale wave disruption (Lee and Butler 2020) and thus the temperature and wind anomalies weaken and gradually descend in altitude (Limpasuvan et al. 2004), much like during the onset of SSWs.



**Vortex intensification** events (VIs) are the result of periods with anomalously low wave activity in the stratosphere allowing for radiative cooling to establish a stronger polar vortex with stronger westerly winds (Limpasuvan et al. 2005). They are defined when  $U_{10,60}$  exceeds  $41.2 \text{ m s}^{-1}$  (Lee and Butler 2020). Unlike SSWs, the growth of the temperature and wind anomalies is much weaker and slower as it is reliant on radiative cooling processes rather than the relatively rapid wave forcing that induces negative wind anomalies. As such, the decay of strong vortex events is quicker than the equivalent decay of SSWs as, in essence, its forcing mechanisms are the reverse, with wave forcing ending the intensification rather than inducing it. One similarity in both event types, however, is that the temperature and wind anomalies always descend through the stratosphere (Limpasuvan et al. 2005).

Annual **final stratospheric warming** events (FSWs) are when the polar stratosphere reverses into its summer easterly state and the wintertime polar vortex breaks down (Black and McDaniel 2007, Butler et al. 2020). It is defined to be the first day of easterly  $U_{10,60}$  that is not followed by a recovery to westerlies for at least 10 consecutive days until the following winter season. FSW events are primarily radiatively driven as the sun returns to the Northern Hemisphere pole, but they can also be driven by dynamic wave forcing as with major SSWs (Lee and Butler 2020). The stratospheric westerly zonal winds decelerate as strong easterly anomalies develop in the mid-stratosphere that strengthen and move downward through the lower stratosphere and into the tropopause (Black and McDaniel 2007).

The **North Atlantic Oscillation** (NAO) is a measure of the strength of the Icelandic Low and the Azores High (IPCC 2007) and the large-scale oscillation of atmospheric mass between the two pressure systems (Trigo et al. 2002). The resultant climate variability is of interest during winter especially. During positive (negative) NAO phases, there is a strengthened (weakened) wintertime meridional pressure gradient as both the Icelandic low-pressure centre and the high-pressure centre over the Azores are enhanced (weakened) (Hurrell et al. 2001). As a result, under positive NAO conditions, the westerly wind field over the North Atlantic is strengthened, advecting warm, moist air to the northeast, producing warmer, wetter conditions over northern Europe and drier conditions over southern Europe. Meanwhile, stronger northerly winds bring cold conditions to Greenland and north-eastern Canada. Conversely, under negative NAO conditions, the weakened pressure gradient leads to the advection of warm, moist Atlantic air over Greenland and Canada and cold, dry Arctic air over northern Europe (Trigo et al. 2002, Hurrell et al. 2003).

## 2.1. Stratospheric Warming Events

February 2018 SSW Onset (07/02/2018 – 16/02/2018) and Decline (23/02/2018 – 04/03/2018)

A Northern Hemisphere major sudden stratospheric warming event began on 12 February 2018 (Karpechko et al. 2018, Lee and Butler 2020, Butler et al. 2020). In this case, the  $U_{10,60}$  reversal was the result of a rapid deceleration in wind speed due to a strongly amplified wavenumber 2 planetary-scale wave pattern. It was also accompanied by an abrupt split of the polar vortex into two smaller vortices. The resultant anomalous high pressure over the

polar stratosphere had a downward influence that reached the troposphere within a week and, along with bringing the descending easterly winds, shifted the North Atlantic storm track equatorward (Butler et al. 2020). In conjunction with a strengthened negative NAO among other factors, these conditions led to cold easterly airflow from central Russia across much of Europe in the last week of February into early March. The so called “Beast from the East” was the physical manifestation of this weather system felt over the British Isles from 24 February to 4 March in the form of unseasonably low temperatures and significant snowfall (Greening and Hodgson 2019). The  $U_{10,60}$  reversal persisted for 19 days with a minimum  $U_{10,60}$  of  $-24 \text{ m s}^{-1}$  (Lee and Butler 2020) reached on 15 February (Karpechko 2018).

During the onset period, it is expected that there might be some differences in the upper-level dispersion patterns using  $\text{Met}_P$  versus using  $\text{Met}_{70}$  ahead of the  $U_{10,60}$  reversal because the decrease in velocity descends from above and the SSW is only defined once the reversal reaches  $\sim 30 \text{ km}$  which is approximately where the change in met data begins as well. However, with the abrupt start to this event, it is possible more differences will be seen during the decline period as the winds begin to recover from above, coinciding with the cold surface weather.

#### *January 2019 SSW Onset (28/12/2018 – 06/01/2019) and Decline (15/01/2019 – 24/01/2019)*

Unlike the February 2018 SSW event, the onset of the major SSW event on 2 January 2019 was more gradual, with the polar vortex beginning to weaken in early December 2018 as the amplitude of a wavenumber 1 planetary wave pattern slowly increased to above-average values. Initially, this led to an elongation and displacement of the stratospheric polar vortex, before the daily-mean  $U_{10,60}$  became easterly on 2 January 2019 and the vortex split into two smaller vortices (Lee and Butler 2020, Butler et al. 2020). The magnitude of the wind reversal was smaller than the February 2018 event, reaching a minimum of  $-10.2 \text{ m s}^{-1}$  on 10 January, but the easterlies persisted for a similar length of time, 21 days (Lee and Butler 2020). There was a weaker stratosphere-troposphere coupling following the SSW as well, with no influence on the NAO phase and only a slight surface influence over the northern U.S. and Canada at the end of January, giving a week of anomalous cold temperatures (Butler et al. 2020).

Given the smaller magnitude of the wind reversal for this SSW, it is possible that any differences between using  $\text{Met}_P$  and  $\text{Met}_{70}$  may be smaller throughout the event than during the February 2018 SSW. However, with the more gradual onset, there may be more discernible differences in the direction of upper-level dispersal ahead of the  $U_{10,60}$  reversal. During the decline stage, as westerlies descend from above, differences in the dispersal direction are again expected.

#### *April 2019 FSW (18/04/2019 – 27/04/2019)*

In 2019, the FSW transitioning into summer conditions occurred on 23 April. It had a substantial dynamic component with high wave activity preceding the  $U_{10,60}$  reversal (Lee and Butler 2020). With this wind reversal also being driven by the gradual radiative warming of the sun, it is possible that, although the final shift in wind direction may occur as rapidly as during the SSW events, the differences in wind direction between  $\text{Met}_P$  and  $\text{Met}_{70}$  may be smaller.

## **2.2. Vortex Recovery and Intensification Events**

*2019 Stratospheric Polar Vortex Recovery (28/01/2019 – 06/02/2019 and 16/02/2019 – 25/02/2019)*

The stratospheric conditions following the 2019 SSW during vortex recovery can be considered to be fairly typical in regard to wind strength and direction for winter in the Northern Hemisphere. Although, with  $U_{10,60}$  still rising, the conditions might be considered closer to early winter when the polar vortex is first forming and strengthening. There should be no major changes in wind direction with height so any differences between the ash clouds modelled using the two met options are expected to be in the distance travelled rather than the direction.

*March 2019 Polar Vortex Intensification (04/03/2019 – 13/03/2019 and 11/03/2019 – 20/03/2019)*

Following on from the 2019 SSW and vortex recovery, the stratospheric polar vortex strengthened further to produce a vortex intensification event on 5 March 2019. The event peaked on 12 March when  $U_{10,60}$  reached  $52.2 \text{ m s}^{-1}$ . Such an intensification occurred after the January 2019 SSW event because, combined with the anomalous easterly winds at lower levels preventing upwards propagation of planetary waves allowing for the vortex recovery in the first place, the SSW occurred relatively early in winter. As a result, minimal solar radiation reached the Arctic in the weeks following, allowing for further enhanced radiative cooling (Lee and Butler 2020). With the February 2018 SSW occurring later in the season, and producing a stronger wind reversal to recover from, a similar intensification could not have happened afterwards.

Similar to the regular recovery period, it is expected that most differences in the spread of the ash cloud will be in the distance travelled from the volcano and not the direction. With higher magnitude wind speeds involved, it is likely that the differences will be more prominent than during the normal recovery period, however. In addition, the increased dispersal may favour the plume simulated using Met<sub>70</sub> leading up to the peak wind speeds but favour the plume simulated using Met<sub>P</sub> after the fact as the winds first accelerate slowly and then decelerate rapidly from above.

## **2.3. Summer**

*Summer 2018 (07/08/2018 – 16/08/2018)*

The relatively weak easterlies present in the summer stratosphere prevent the propagation of tropospheric planetary-scale waves from influencing upper-level winds (Lee and Butler 2020) and lead to more consistent stratospheric conditions than in winter. As a result, fewer differences in the spread of the ash cloud when comparing runs using Met<sub>P</sub> and Met<sub>70</sub> are expected, with any differences that do occur being the result of the increase in wind speed with altitude. It should be noted that during this period an ex-hurricane passes through the region. However, with the meteorological conditions remaining the same at those levels affected by synoptic scale weather systems, any effect on the dispersion of ash from this system will be confined to the troposphere, below the height of interest.

### 3. Methods

#### 3.1. Meteorological Data Acquisition and Setup

In the current operational VAAC system, only met forecast data for the first 59 MetUM Global vertical levels, up to the 30 km altitude limit, are processed and used for NAME. To run NAME using the actual met forecast data for higher atmospheric layers, the remaining 11 MetUM Global vertical levels must be obtained. All 70 vertical levels of MetUM Global model data are stored centrally by the Met Office and must be downloaded and processed into the correct format for NAME to accept. When accessing data for the case study periods involving 2019 dates, 1-hour averaged surface sensible heat flux values are used in substitution of the normal 3-hour averaged values due to this variable not being stored in the same archive as the rest of the met data for these periods. Unlike in the operational setup, where the most recent forecast is used to initiate NAME, here the first 6 hours (+00, +03, +06) of each forecast cycle (00Z, 06Z, 12Z, 18Z) have been combined together to provide a more accurate representation of the meteorological conditions throughout each case study period.

In order to run NAME using either Met<sub>P</sub> data or Met<sub>70</sub> data for heights above 30 km, the met definition and main input files must be altered appropriately. To persist the met data, Z Max (the maximum height of the model domain) must be increased beyond 30 km to the maximum MetUM data height, equivalent to 80 km, while restricting the accessible vertical grid of met data to the lowest 59 levels (~30 km). This prevents ash particles from disappearing once they reach 30 km, as is the case with the current setup, but forces them to be transported using the last available met data from the 59<sup>th</sup> level for subsequent upper-level dispersion. Then, to use all 70 levels of MetUM data simply requires removing the height limit on the accessible vertical grid of met data in addition to increasing Z Max. The met data files used were the same for both methods to ensure meteorological conditions remained the same below 30 km.

Table 1: NAME model parameter set-up used for case-studies.

Parameter	Value Used
Source Strength	$1.0 \times 10^{13} \text{ g hr}^{-1}$
Source Shape	Cuboid
Particle Size Distribution	Default (See Table 2)
Particle Density	$2300 \text{ kg m}^{-3}$
# Particles	$15,000 \text{ hr}^{-1}$
Horizontal Met Resolution	$0.140625^\circ$ Longitude, $0.09375^\circ$ Latitude
Vertical Met Resolution	Variable, decreasing from ~50 m near the surface to ~2 km at level 59 (~30 km) and ~7 km at level 70 (80 km)
NAME Domain Start	06:00 on Case Study Start Date
Source Release Start	06:00 on Case Study Start Date
NAME Run Duration	210 Hours (8.75 Days)
Horizontal NAME Output Resolution	$0.5625^\circ$ Longitude, $0.375^\circ$ Latitude
Vertical NAME Output Resolution	FL000 to FL550 at 25FL intervals or Total Column Integral
Temporal NAME Output Resolution	6 Hourly from 12:00 on Case Study Start Date

Table 2: NAME's default particle size distribution.

Particle Diameter Range Boundary ( $\mu\text{m}$ )	Cumulative Mass Fraction
0.1	0.0
0.3	0.001
1.0	0.006
3.0	0.056
10.0	0.256
30.0	0.956
100.0	1.0

### 3.2. NAME Setup and Outputs

NAME v8.1 was used to complete the model runs, and, to ensure that the results from this research remain applicable to operational VAAC runs, the default VAAC NAME settings were used where possible (Table 1). The main differences are: i) the constraint on the maximum age of particles was turned off, particles are removed after 6 days in the VAAC system to speed up run times operationally, and ii) a unit source strength of appropriate magnitude was used across all plume heights to allow for easier comparison, while this is normally calculated per event using the Mastin relationship (Mastin et al. 2009, Witham et al. 2020, Beckett et al. 2020). We used the default particle size distribution (Table 2) and particles were released uniformly from the summit height of 2010 m asl to the respective plume heights for each model run. Along with acting as a crude mimicry of umbrella clouds, the more compact 30-35 km plume depth runs help to make identification of differences in dispersion due to upper-level met easier in the case studies where they are used.

Each NAME run was initiated at the source release start time and ran for approximately 9 days to account for the changing conditions apparent in some of the case study periods and to simulate the situation of a prolonged eruption when new dispersion forecasts are made days after the start of an event with updated met forecast data. Detailed volcanic ash information was output over the two vertical resolutions used operationally. Firstly, as an ash air concentration ( $\mu\text{g m}^{-3}$ ) over 'thin' flight level (FL) depths from FL000 to FL550 at 25FL intervals, which were then processed into the thicker operational flight level depths of FL000 to FL200, FL200 to FL350 and FL350 to FL550 by taking the highest concentration from the constituent 'thin' flight levels for each horizontal grid point and applying it to the 'thick' layer. Then, as a total column mass loading ( $\text{g m}^{-2}$ ) over the entire depth of the atmosphere. Both outputs were produced every 6 hours after the source release start time, but they had different averaging periods. The flight level outputs are a 6-hour average to cover the likely position of ash over the entire 6-hour period, while the total column values are a 1-hour average, as their main purpose in a real event is for comparison with satellite observations which requires a shorter validity period.

### 3.3. Statistical Analysis

To consider whether using  $\text{Met}_P$  rather than  $\text{Met}_{70}$  affected the horizontal extent of the simulated ash clouds we calculated the Figure of Merit in Space (FMS), defined as the percentage of overlap between the intersection of both areas of interest and the union of both

areas of interest:

$$FMS = \frac{A_P \cap A_{70}}{A_P \cup A_{70}} \times 100$$

where  $A_P$  is the calculated area of the  $Met_P$  ash cloud with an ash concentration (mass loading) greater than  $200 \mu\text{g m}^{-3}$  ( $0.2 \text{ g m}^{-2}$ ) and  $A_{70}$  is the calculated area of the  $Met_{70}$  ash cloud following the same threshold(s). The  $200 \mu\text{g m}^{-3}$  threshold aligns with the 'low contamination' level used by VAACs London and Toulouse in their supplementary concentration charts produced in addition to the International Civil Aviation Organization (ICAO) Volcanic Ash Advisories (VAA) and Graphics (VAG) (ICAO 2021, CAA 2017), while  $0.2 \text{ g m}^{-2}$  is the equivalent mass loading threshold if a cloud depth of 1 km is assumed. Calculated area is used, rather than the number of model grid points, to account for the varying size of grid boxes with latitude that can be visually misleading in some map projections. FMS values were calculated for each output timestep of each NAME run (Appendix Figure A1). The greater the FMS percentage at a given time, the more similar the total spreads of the two ash clouds are, while the smaller the FMS the more different they are. In order to compare the values from different runs, temporal averages (mean and minimum) of FMS were also calculated, using the timestep values from each event.

To understand how the internal structures of the ash clouds vary when using  $Met_P$  or  $Met_{70}$ , direct grid cell to grid cell comparisons were made to calculate ash concentration and mass loading differences, which were then used to determine the maximum absolute differences for each case study period. This gives an indication to how the higher concentration threshold regions may be affected by the differing meteorological conditions.

## 4. Analysis

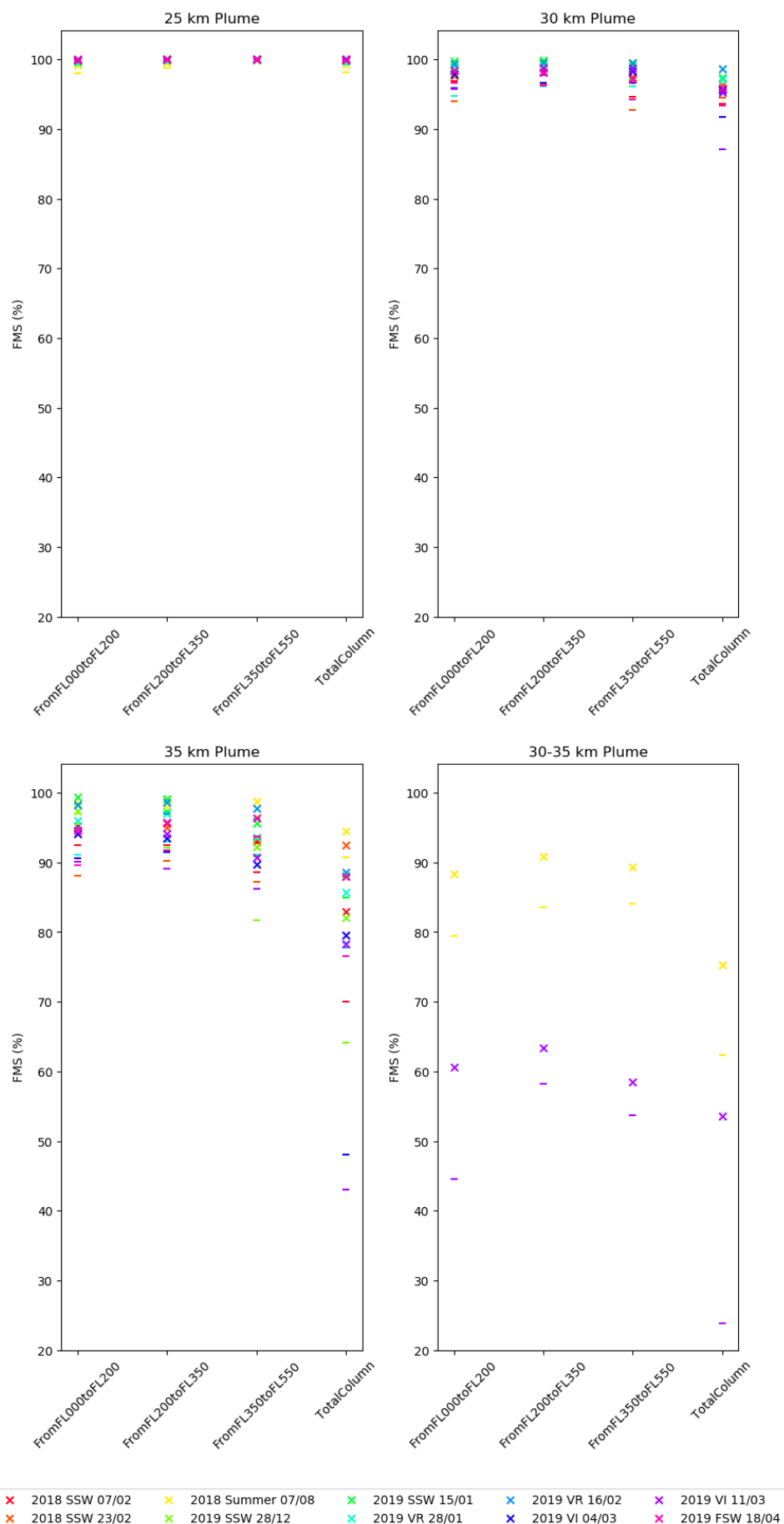
### 4.1. Sensitivity to Plume Height

Figure 3 shows the calculated mean and minimum FMS, across all forecast times, for each of the case studies considered, when the initial plume height is varied. When ash is released exclusively below 30 km, the ash clouds simulated using Met<sub>P</sub> and Met<sub>70</sub> are very similar: for initial plume heights of 25 km every FMS > 98%. As ash is released at altitudes  $\geq 30$  km, the level of agreement between the ash dispersal simulated with Met<sub>P</sub> and Met<sub>70</sub> lessens. When the initial plume heights are 30 km, bordering the met changes around the 59<sup>th</sup> vertical MetUM level, FMS values remain > 87%. The greatest discrepancies between the simulated ash clouds arise when ash is released up to 35 km. When ash is released at all altitudes, from the summit to 35 km, the smallest total column ash mass loading FMS values are < 50%. When ash is released over a limited depth, between 30-35 km, reflective of an umbrella cloud, the FMS values decrease significantly, with the 2019 VI minimum total column FMS value becoming < 25%. This reflects the increasing influence of the differing upper-level met conditions on the dispersal of higher altitude ash. Additionally, we find that the maximum difference in flight level layer ash concentrations and total column ash mass loadings increases as plume height increases (Table 3). Another difference seen in the change from 25 km to 30 km plume heights is the distribution of the differences. When ash is released up to 25 km, differences between the two simulations occur evenly throughout the ash cloud (Appendix Figure A2), whereas when ash is released up to 30 km, distinct regions favouring one approach start to appear (Appendix Figure A3). The size of the differences begins to decrease with increasing distance from the source as well, as particles sediment to lower atmospheric layers where the met conditions are identical.

*Table 3: The maximum differences in simulated flight level layer ash concentration and total column ash mass loading between the Met<sub>70</sub> and Met<sub>P</sub> simulated ash clouds for each case study and plume height. These are based on the absolute concentration differences from any of the three flight level layers and the absolute total column mass loading differences.*

Case Study	25 km		30 km		35 km	
	Flight Level Layers ( $\mu\text{g m}^{-3}$ )	Total Column ( $\text{g m}^{-2}$ )	Flight Level Layers ( $\mu\text{g m}^{-3}$ )	Total Column ( $\text{g m}^{-2}$ )	Flight Level Layers ( $\mu\text{g m}^{-3}$ )	Total Column ( $\text{g m}^{-2}$ )
2018 SSW 07/02	3.1e+3	2.0e+1	4.4e+3	7.3e+1	5.7e+3	9.4e+2
2018 SSW 23/02	1.4e+2	3.1e-1	4.3e+3	1.3e+2	6.4e+3	2.5e+3
2018 Summer 07/08	1.9e+3	5.7e+0	5.4e+3	3.0e+2	2.1e+4	4.8e+3
	Shallower release depth 30-35 km				1.2e+5	3.2e+4
2019 SSW 28/12	1.2e+3	7.1e+0	1.5e+3	1.0e+2	3.3e+3	9.6e+2
2019 SSW 15/01	4.9e+2	1.1e+0	4.1e+3	7.1e+2	1.1e+4	8.0e+3
2019 VR 28/01	1.8e+3	8.5e+0	5.7e+3	9.6e+1	6.1e+3	1.1e+3
2019 VR 16/02	3.3e+2	1.8e+0	7.2e+3	5.2e+1	9.9e+3	6.7e+2
2019 VI 04/03	5.2e+2	2.9e+0	1.9e+3	3.3e+1	3.3e+3	3.0e+2
2019 VI 11/03	6.3e+2	1.2e+0	2.6e+2	2.2e+1	4.9e+3	2.4e+2
	Shallower release depth 30-35 km				1.1e+4	1.5e+3
2019 FSW 18/04	7.2e+2	1.8e+0	7.0e+3	2.2e+2	7.5e+3	3.2e+3

Figure 3: Mean (crosses) and minimum (dashes) FMS values for each case study for varying plume height, calculated using the  $200 \mu\text{g m}^{-3}$  threshold over the operational flight level layers and the  $0.2 \text{ g m}^{-2}$  threshold for the total column.





## 4.2. Sensitivity to Stratospheric Conditions

We now consider the high-altitude release scenarios more closely. There are many similarities in how differences in ash dispersal present themselves across the different met scenarios when ash is released up to 35 km:

- The ash clouds simulated using Met<sub>70</sub> are broader than their Met<sub>P</sub> counterpart. Consequently, ash clouds simulated using Met<sub>P</sub> have higher ash mass loadings and concentrations through the centre of the ash clouds.
- FMS values tend to be lower, indicating greater differences in the predicted horizontal spread of the ash clouds, when the differences in the predicted ash mass loadings and concentrations are small (Figure 4). Whereas, when FMS values are high, and thus the horizontal spreads are similar, the maximum ash mass loading and concentration differences are larger.

Despite these similarities, the events still have their own quirks.

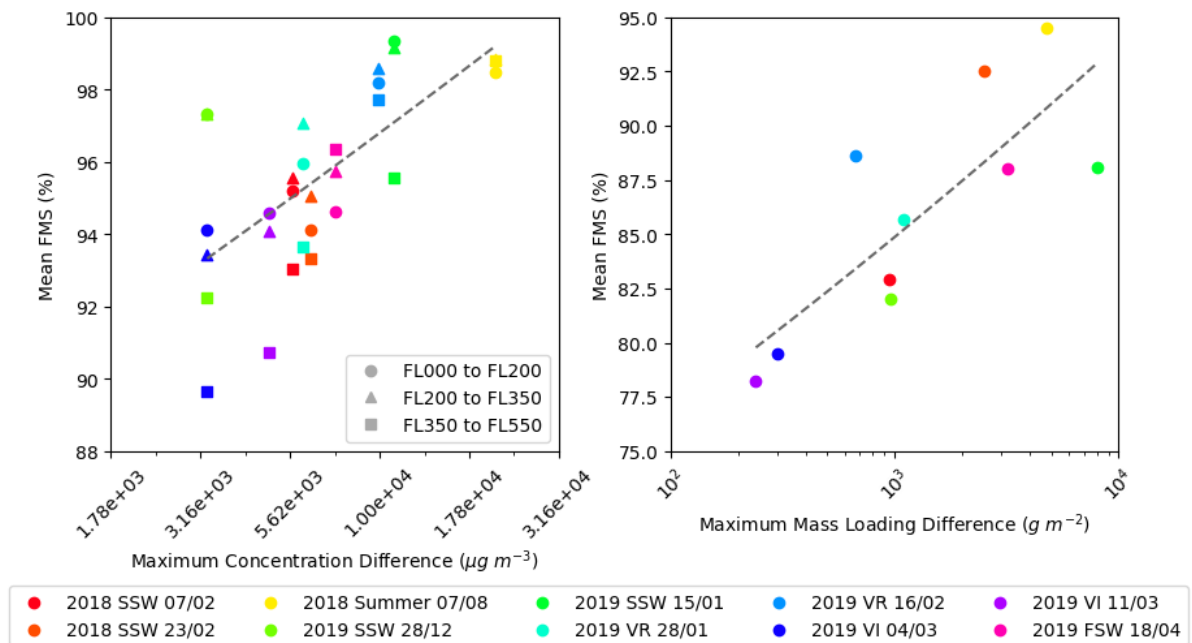
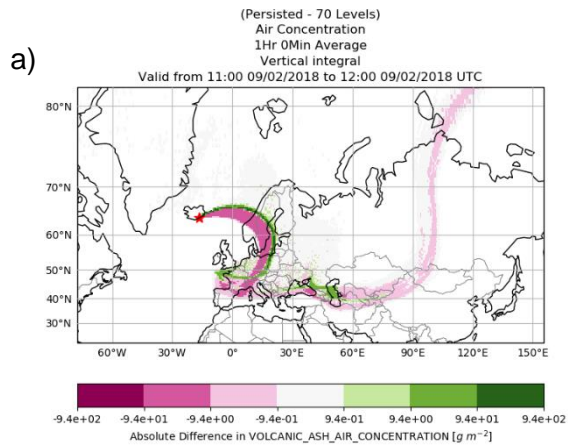


Figure 4: a) Mean FMS for each flight level layer against the maximum ash concentration difference and b) mean total column FMS against the maximum ash mass loading difference, for each case study. The dashed grey lines show simple linear interpolations of the relationships.

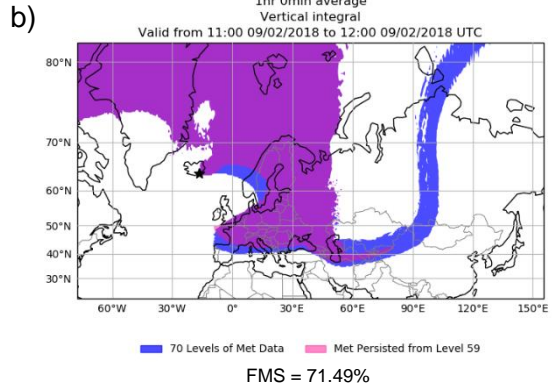
### 4.2.1. Stratospheric Warming Events

During the 2018 SSW event, ahead of the  $U_{10,60}$  reversal, both plumes initially disperse north-east from Öraefajökull (Figure 5), with a more eastward spread apparent above 30 km implied by the regions of large mass loading differences in Figure 5a. There is also a noticeable plume streak travelling further east than the rest of the ash cloud at around  $40^\circ\text{N}$  in both simulations (Figure 5b). However, when using Met<sub>70</sub>, this region of ash is spread further and more broadly than when using Met<sub>P</sub>, leading to the low FMS of 71%. Based on the differences in dispersal of this region of ash between the two scenarios and the large differences in predicted mass

Comparison between 70 Levels of Met and Met Persisted from Level 59



Area Comparison of Regions with  
Volcanic Ash Air Concentrations  $> 0.2\ g\ m^{-2}$



Comparison between 70 Levels of Met and Met Persisted from Level 59

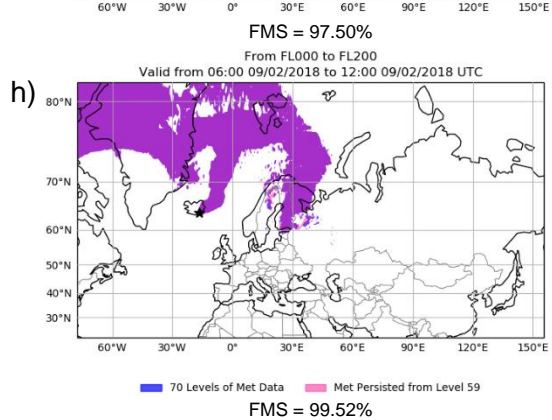
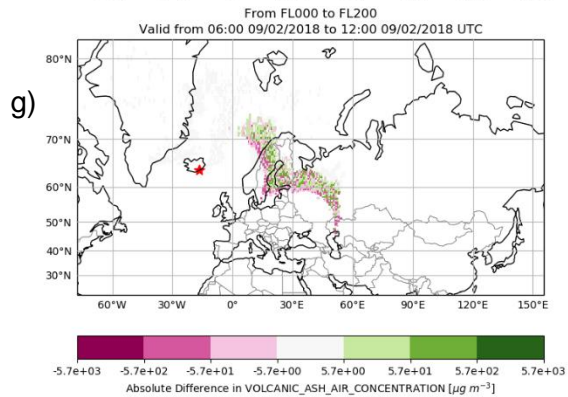
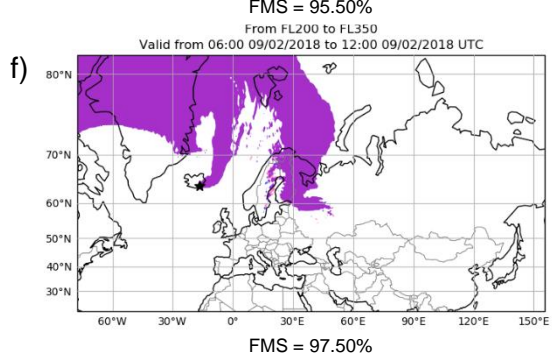
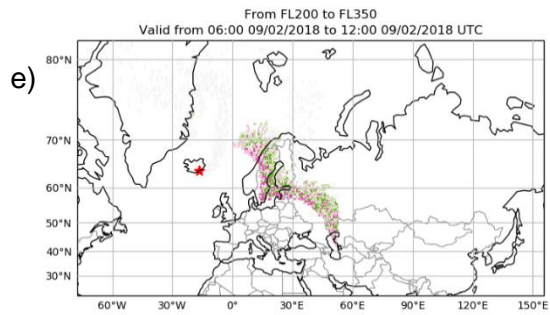
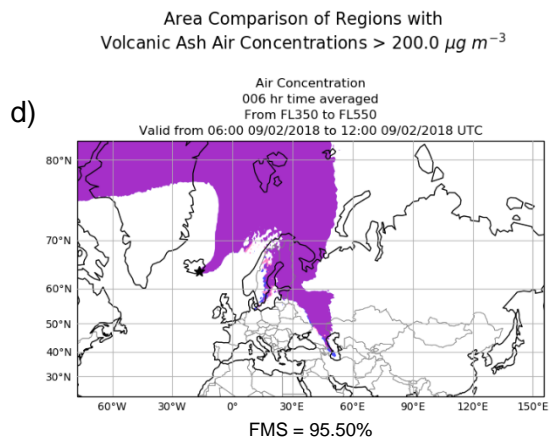
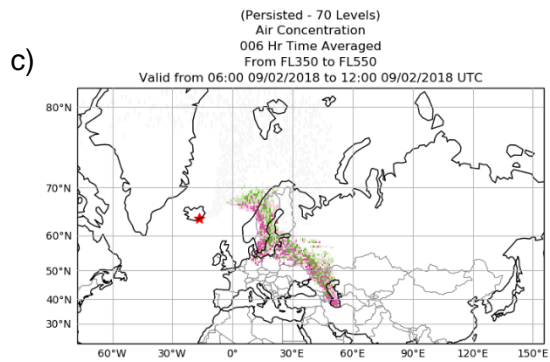
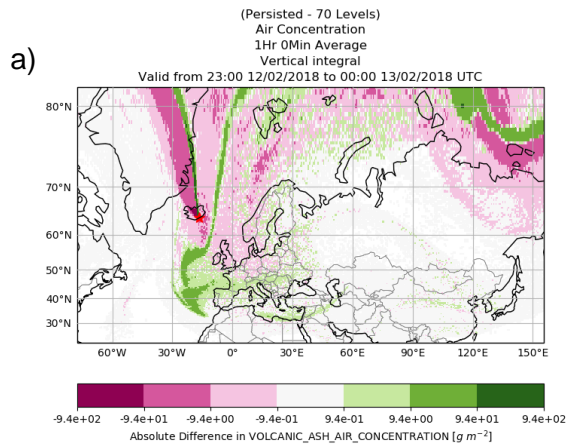
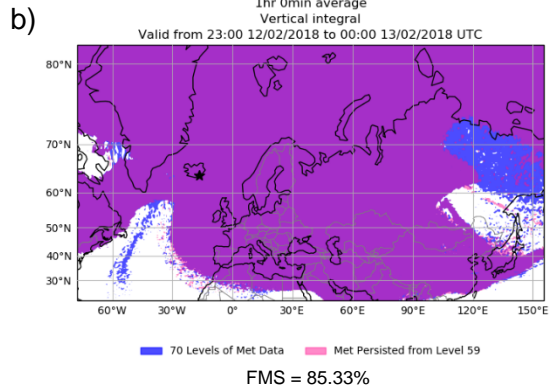


Figure 5: To compare simulated ash clouds produced using Met<sub>P</sub> and Met<sub>70</sub> during the 2018 SSW 07/02 run at T+54 (12:00 09/02/2018) for a plume height of 35 km. (a) Total column mass loading differences, (b) ash cloud area comparison for mass loading values above  $0.2\ g\ m^{-2}$ , (c, e, g) flight level layer concentration differences and (d, f, h) ash cloud area comparison for concentrations above  $200\ \mu g\ m^{-3}$ . Note: All flight level layers are below 30 km, the contour scales differ for the total column mass loading and flight level layer differences plots, and in the area comparison plots the purple region represents an ash cloud area forecast by both met scenarios.

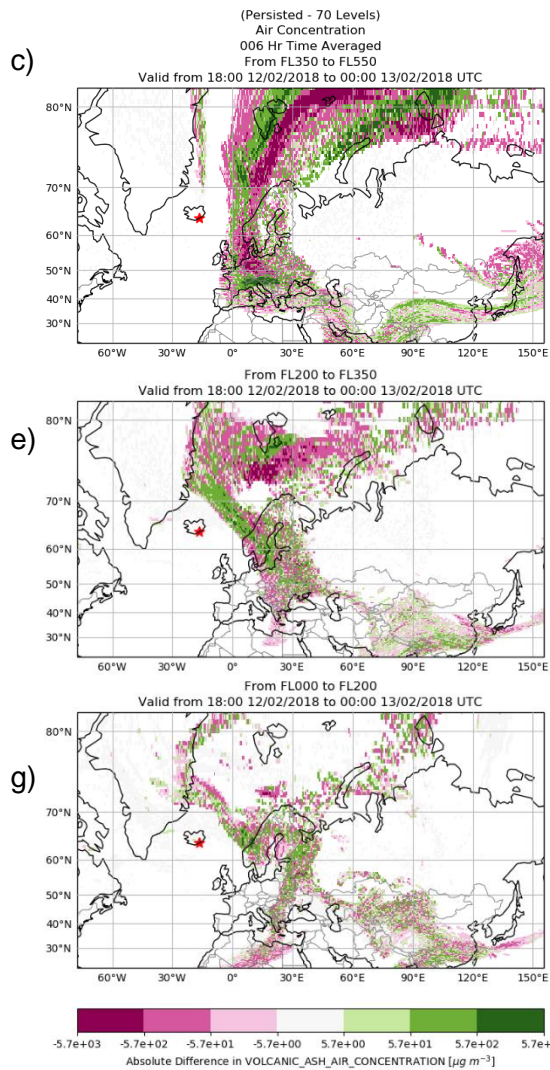
Comparison between 70 Levels of Met and Met Persisted from Level 59



Area Comparison of Regions with  
Volcanic Ash Air Concentrations  $> 0.2\ g\ m^{-2}$



Comparison between 70 Levels of Met and Met Persisted from Level 59



Area Comparison of Regions with  
Volcanic Ash Air Concentrations  $> 200.0\ \mu g\ m^{-3}$

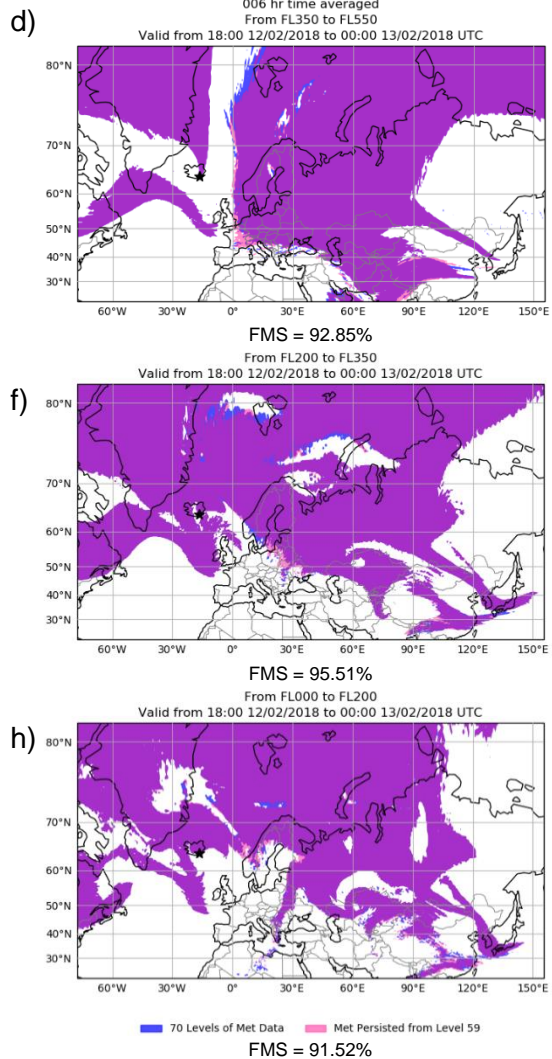


Figure 6: As in Figure 5, but for  $T+138$  (23:00 12/02/2018 to 00:00 13/02/2018 and 18:00 12/02/2018 to 00:00 13/02/2018).

loadings, it can be inferred that this streak occurs above 30 km, as a result of the differing upper-level met conditions. Nevertheless, having occurred prior to the  $U_{10,60}$  reversal on the 12<sup>th</sup> and within the mid-latitudes, this difference in dispersal is not directly related to the SSW event and is thus unexpected. Equally, unlike other mass loading differences throughout the central ash cloud region, the relatively smaller magnitude differences associated with this plume streak do not transfer down to the flight level layers (Figure 5c,e,g). The concentration differences that are seen in the flight level layers are less defined than their total column mass loading equivalents, but their positions coincide well with the locations of the largest magnitude mass loading differences.

Leading up to the daily-mean  $U_{10,60}$  direction reversal on the 12<sup>th</sup>, both ash clouds gradually spread further north with a westward tilt showing in the upper levels by the latter part of the 12<sup>th</sup> (Figure 6a), as expected with the shift to easterly stratospheric winds. At this time, differences in the dispersal of the two clouds can be seen again, with Met<sub>70</sub> spreading ash further to the west in a wider band, while Met<sub>P</sub> produces higher ash mass loadings more centrally through the ash cloud, but over a narrower region. This is indicative of the upper-level winds becoming easterly earlier in Met<sub>70</sub> than in Met<sub>P</sub> and there being less variation in the dispersal direction of ash above 30 km when using Met<sub>P</sub> due to the persisted wind directions at such altitudes. These differences do not affect the predicted areal extent of ash mass loadings  $> 0.2 \text{ g m}^{-2}$ , shown in Figure 6b, because the underlying ash clouds at lower altitudes have spread further into this region as well (Figure 6c,e,g), leading the higher concentrations of upper-level ash to increase the central mass loadings only. However, earlier dispersed differences along the fringes of the ash clouds do have an influence on the size of the Met<sub>70</sub> cloud above  $0.2 \text{ g m}^{-2}$  (Figure 6b). Similarly, it is these earlier differences that show the greatest influence in the flight level layers at this time (Figure 6c,e,g), affecting the ash cloud areas as well (Figure 6d,f,h). The total column FMS values for this period (Figure 5b and Figure 6b, Appendix Figure A1a) are seen to increase with time as the ash clouds increase in size and develop similar horizontal extents. Meanwhile, in the flight level layers, the opposite is seen, with FMS values decreasing with time in each of the layers (Figure 5d,f,h and Figure 6d,f,h, Appendix Figure A1b-d).

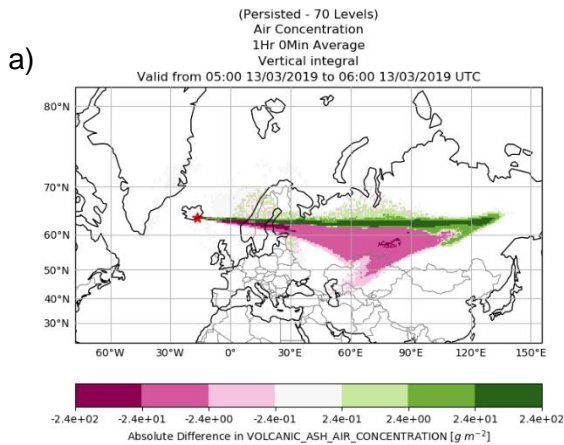
During the 2019 SSW event, the Met<sub>70</sub> ash cloud similarly reacts to the initial change in wind direction to easterlies earlier than the Met<sub>P</sub> cloud (Appendix Figure A4). After peak  $U_{10,60}$  speeds are reached in both events, the Met<sub>70</sub> clouds react to the subsequent weakening of the SSW earlier again, with the mass loading differences showing the earlier shift in dispersal to the east (Appendix Figure A5a and Appendix Figure A6a). During the 2019 FSW event, the earlier shift to easterlies in Met<sub>70</sub> is seen to have a similar impact on the dispersal differences to both SSW events (Table 3, Figure 3, Appendix Figure A1). In this period, the extra Met<sub>70</sub> spreading is accompanied by Met<sub>P</sub> producing additional spreading outside the shared dispersal area as well. However, only during the 2018 SSW onset case is there additional Met<sub>70</sub> spreading independent from the main dispersal direction (Figure 5a-b).

#### **4.2.2. Vortex Recovery and Intensification Events**

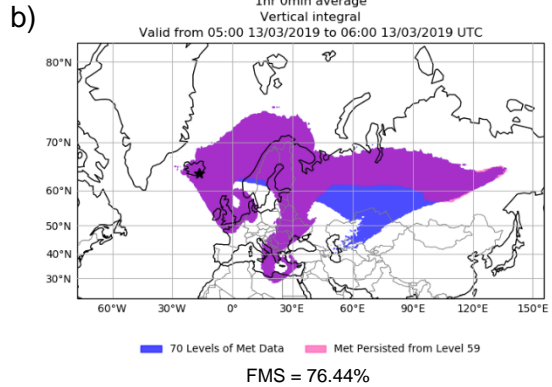
During the later period of the 2019 vortex intensification event, the plumes in both high-release



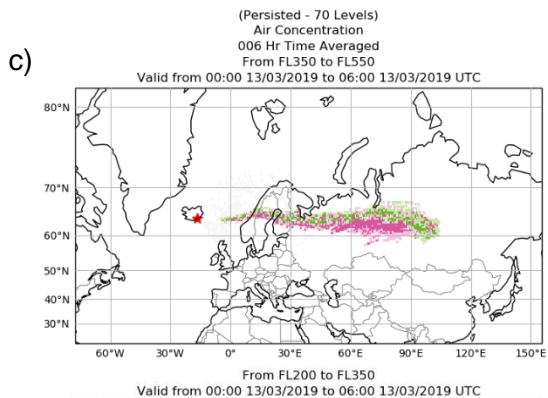
Comparison between 70 Levels of Met and Met Persisted from Level 59



Area Comparison of Regions with  
Volcanic Ash Air Concentrations  $> 0.2\ g\ m^{-2}$



Comparison between 70 Levels of Met and Met Persisted from Level 59



Area Comparison of Regions with  
Volcanic Ash Air Concentrations  $> 200.0\ \mu g\ m^{-3}$

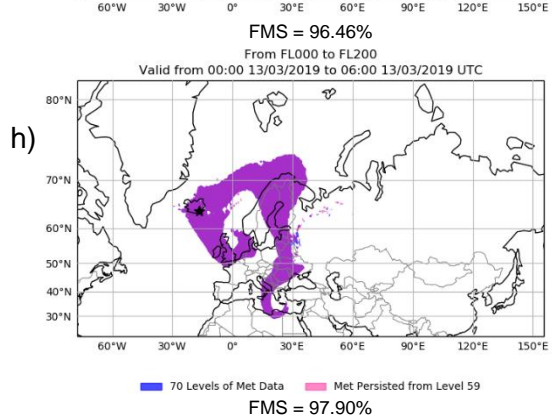
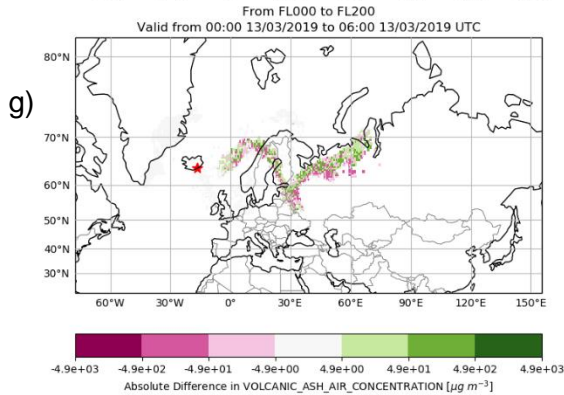
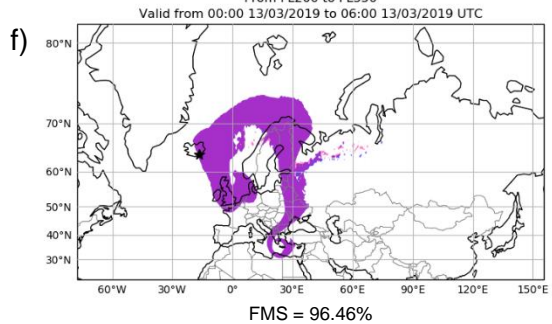
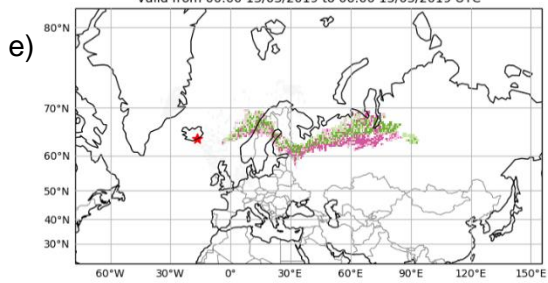
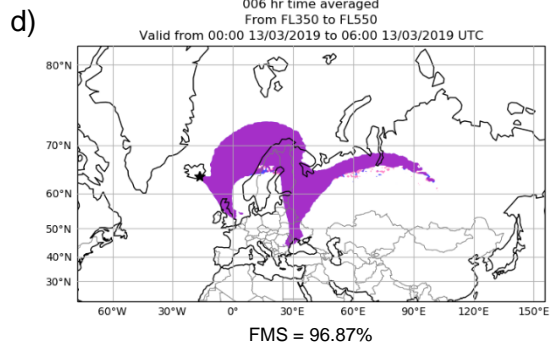
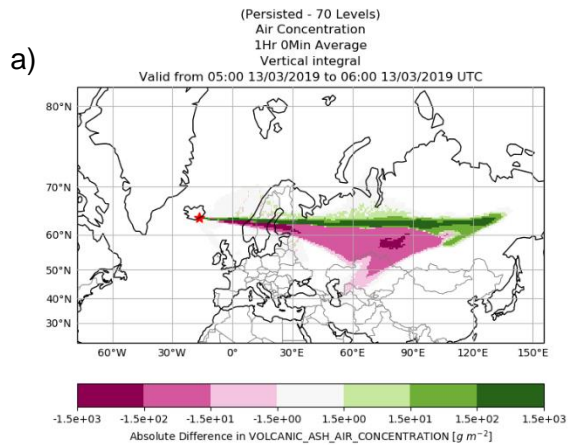
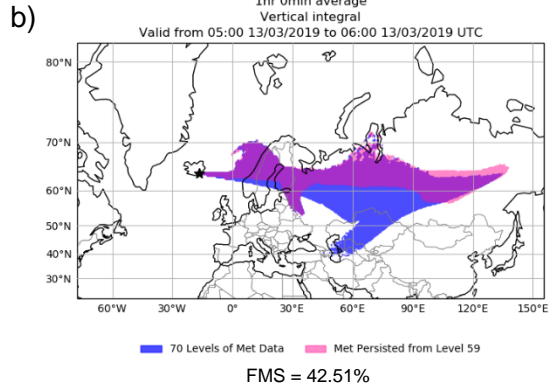


Figure 7: To compare simulated ash clouds produced using Met<sub>P</sub> and Met<sub>70</sub> during the 2019 VI 11/03 run at T+48 (06:00 13/03/2019) for a plume height of 35 km. (a) Total column mass loading differences, (b) ash cloud area comparison for mass loading values above  $0.2\ g\ m^{-2}$ , (c, e, g) flight level layer concentration differences and (d, f, h) ash cloud area comparison for concentrations above  $200\ \mu g\ m^{-3}$ . Note: All flight level layers are below 30 km, the contour scales differ for the total column mass loading and flight level layer differences plots (and differ from Figures 5-6), and in the area comparison plots the purple region represents an ash cloud area forecast by both met scenarios.

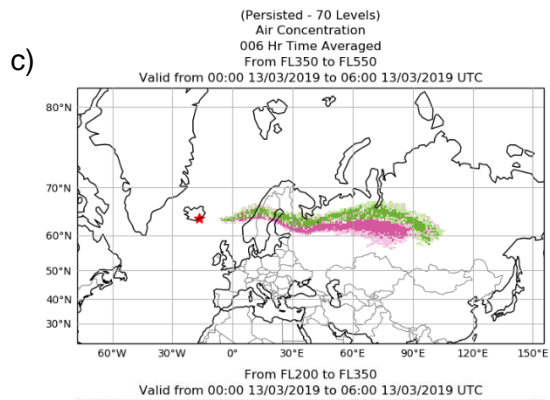
Comparison between 70 Levels of Met and Met Persisted from Level 59



Area Comparison of Regions with  
Volcanic Ash Air Concentrations  $> 0.2\ g\ m^{-2}$



Comparison between 70 Levels of Met and Met Persisted from Level 59



Area Comparison of Regions with  
Volcanic Ash Air Concentrations  $> 200.0\ \mu g\ m^{-3}$

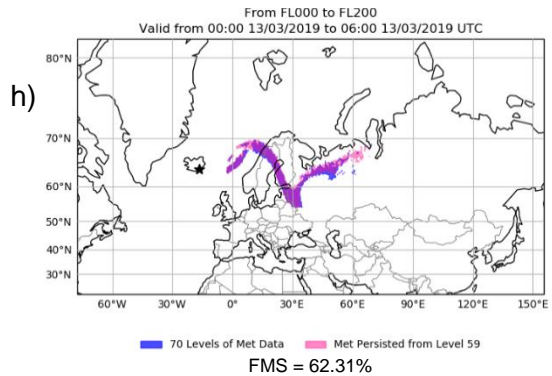
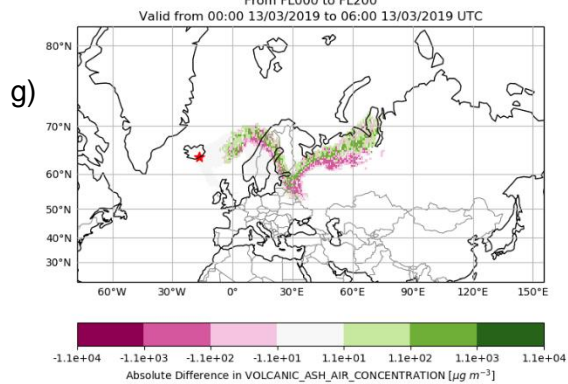
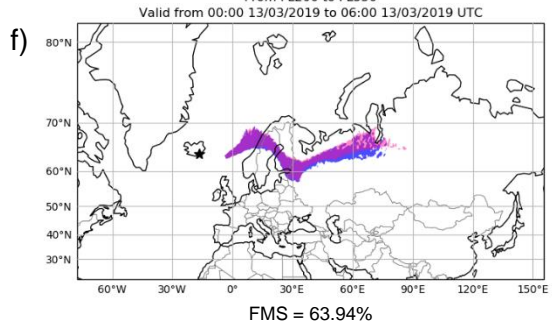
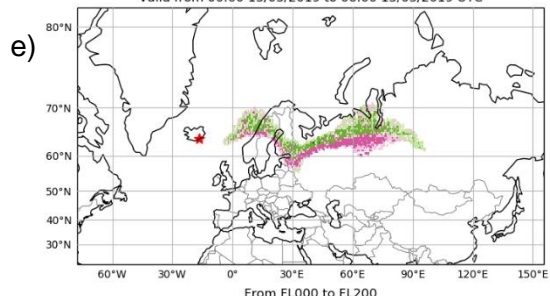
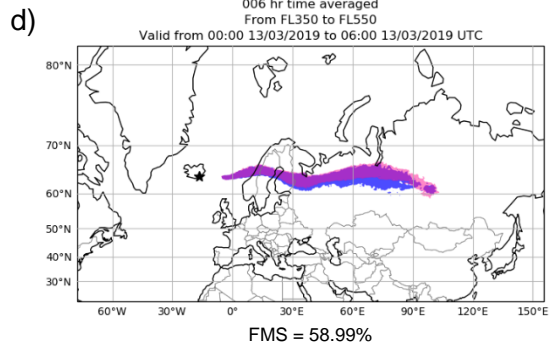


Figure 8: As in Figure 7, but for a release between 30-35 km only, rather than from the summit to 35 km. Note: All flight level layers are below 30 km, the contour scales differ for the total column mass loading and flight level layer differences plots (and differ from Figure 7), and in the area comparison plots the purple region represents an ash cloud area forecast by both met scenarios.

scenarios disperse to the east throughout the total column depth (Figure 7 and Figure 8). With the peak in  $U_{10,60}$  occurring during the 12<sup>th</sup>, by T+48 the Met<sub>70</sub> winds have begun to rapidly weaken from above while the Met<sub>P</sub> winds remain equal to the now faster 30 km winds. This can be seen in the composition of the mass loading differences in Figure 7a and Figure 8a, where a region of Met<sub>P</sub> biased ash is leading the eastward dispersal. While this ash does not influence the total column ash cloud areas in the summit to 35 km releases (Figure 7b), it does affect the ash cloud areas in the limited depth releases (Figure 8b). Conversely, the additional southward spread produced when modelling with the more varied Met<sub>70</sub> winds shows similarly in both release scenarios, occurring over a region without any significant concentrations of ash at lower levels (Figure 7c-h and Figure 8c-h).

In addition to increasing the size of the Met<sub>P</sub>-only and Met<sub>70</sub>-only ash cloud areas created by the differences in ash dispersal, the removal of ash emissions at lower levels in the limited depth releases reduces the size of the shared ash cloud area (Figure 8). This means that while the changes to the Met<sub>P</sub>-only and Met<sub>70</sub>-only ash cloud areas only marginally increase  $A_P \cup A_{70}$ ,  $A_P \cap A_{70}$  shrinks considerably, amplifying the decrease in FMS from 76% to 43%. Additionally, since the mass eruption rate has not been changed for the limited depth releases, the ash previously released below 30 km is also released above 30 km. Thus, the ash mass loading and concentration differences are larger than those seen for the summit to 35 km releases. While this has a limited effect on the distribution of total column ash mass loading differences and areal extents, it does affect the flight level layer distributions. It can be seen in the limited depth releases (Figure 8d,f,h) that the ash cloud area with concentrations  $> 200 \mu\text{g m}^{-3}$  stretches further east in all three flight level layers than in the summit to 35 km releases (Figure 7d,f,h). Moreover, the extent of the two disparate ash cloud regions increases with this change in overall spread as well, again leading to decreased FMS values from ~97% for the summit to 35 km releases to ~60% for the limited depth releases.

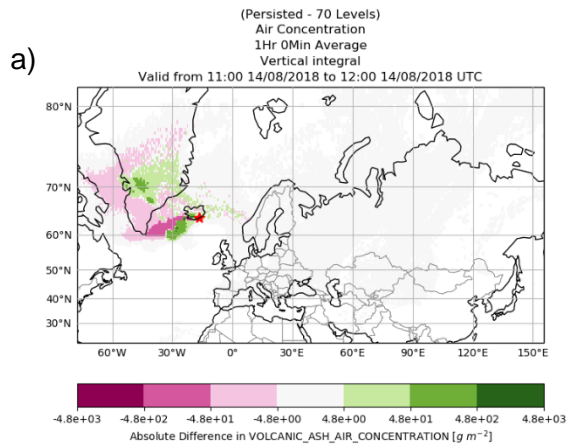
Prior to the peak  $U_{10,60}$  speeds occurring during the 2019 vortex intensification event, because the Met<sub>70</sub> winds increase in magnitude earlier than the Met<sub>P</sub> winds, the Met<sub>70</sub> ash cloud disperses further east (Appendix Figure A8a-b). Likewise, during the vortex recovery after the 2019 SSW, the Met<sub>70</sub> winds strengthen earlier than the Met<sub>P</sub> winds as well, resulting in the Met<sub>70</sub> ash clouds dispersing further east (Appendix Figure A9 and Appendix Figure A10). In the earlier stages of vortex recovery (Appendix Figure A9a) it can also be seen that Met<sub>P</sub> is still lagging in the shift from easterlies to westerlies close to the source.

#### **4.2.3. Summer**

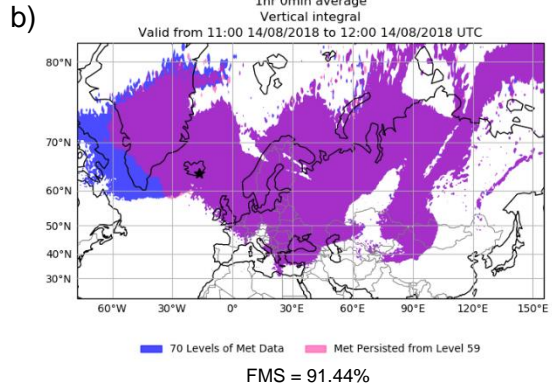
The 2018 summer case study period shows the smallest differences in total column horizontal spread (Figure 3 and Figure 4, Figure 9), but the largest flight level layer ash concentration differences (Table 3 and Figure 4) for the summit to 35 km releases. The differences, and thus the implied upper-level dispersal, are mostly constrained to the west of Iceland where the summertime stratospheric easterlies that strengthen with height disperse the ash further in the Met<sub>70</sub> simulation. As with the vortex intensification case, when a limited depth release is used, the FMS values fall and the mass loading and concentration differences increase (Table 3, Figure 3). However, the changes here appear to mostly be the result of the reduced shared



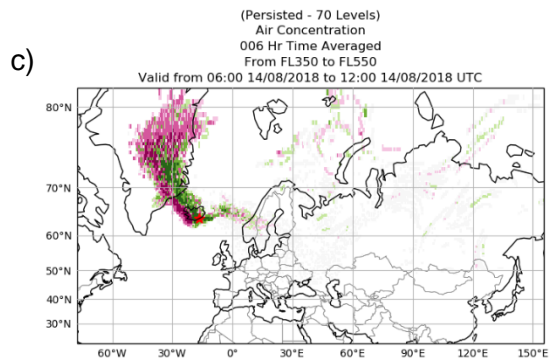
Comparison between 70 Levels of Met and Met Persisted from Level 59



Area Comparison of Regions with  
Volcanic Ash Air Concentrations  $> 0.2\ g\ m^{-2}$



Comparison between 70 Levels of Met and Met Persisted from Level 59



Area Comparison of Regions with  
Volcanic Ash Air Concentrations  $> 200.0\ \mu g\ m^{-3}$

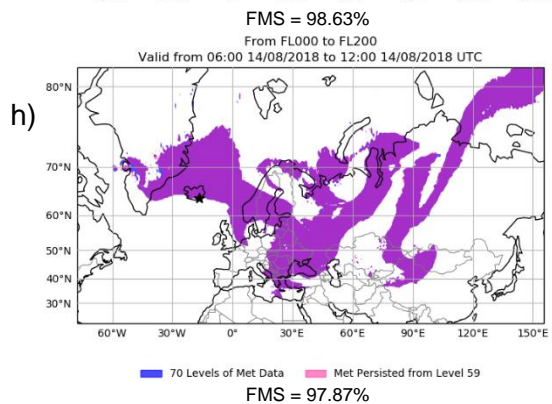
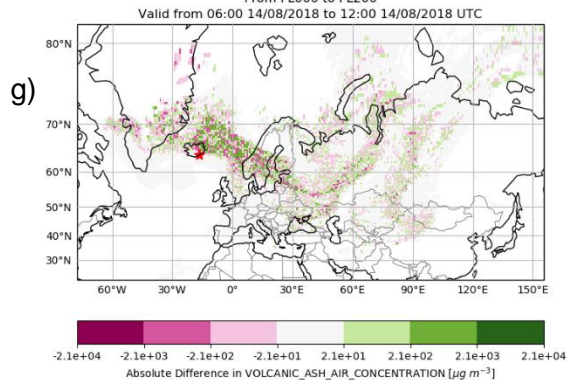
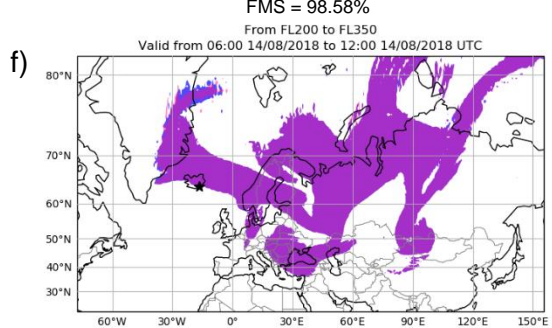
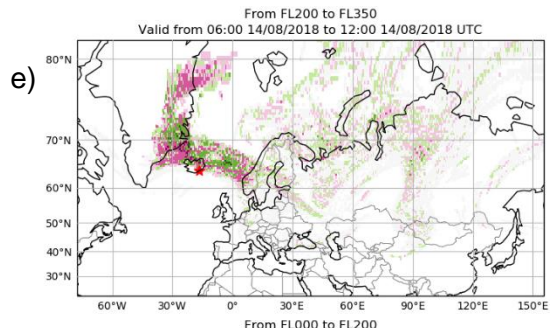
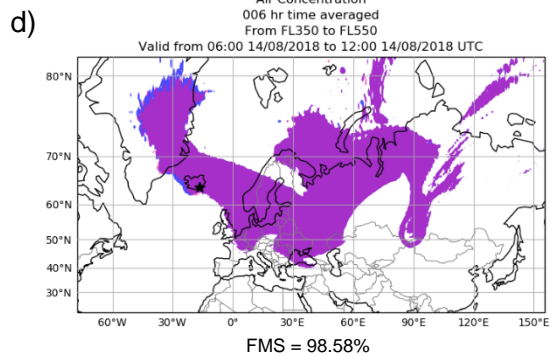
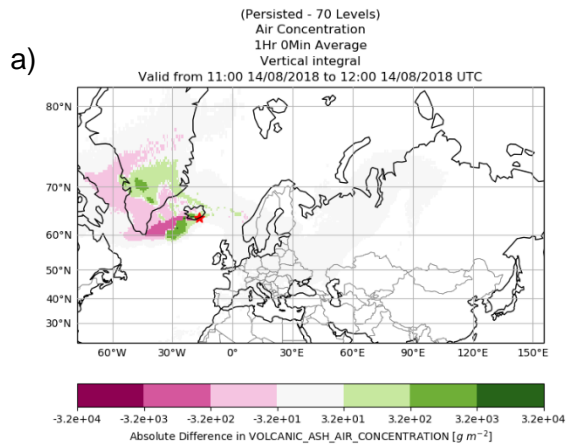


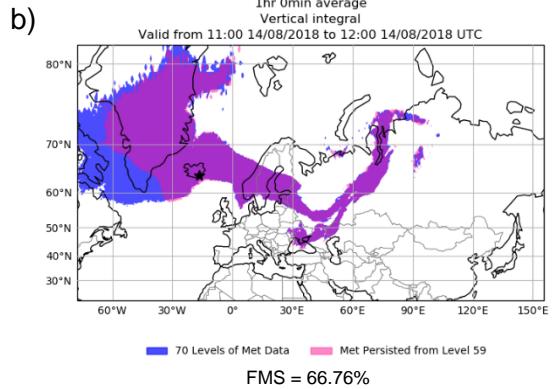
Figure 9: To compare simulated ash clouds produced using Met<sub>P</sub> and Met<sub>70</sub> during the 2018 Summer 07/08 run at T+174 (12:00 14/08/2018) for a plume height of 35 km. (a) Total column mass loading differences, (b) ash cloud area comparison for mass loading values above  $0.2\ g\ m^{-2}$ , (c, e, g) flight level layer concentration differences and (d, f, h) ash cloud area comparison for concentrations above  $200\ \mu g\ m^{-3}$ . Note: All flight level layers are below 30 km, the contour scales differ for the total column mass loading and flight level layer differences plots (and differ from Figures 5-8), and in the area comparison plots the purple region represents an ash cloud area forecast by both met scenarios.



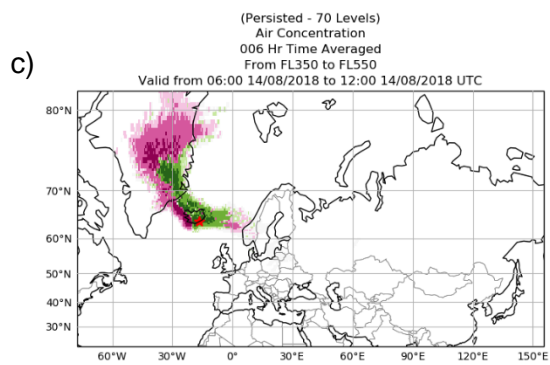
Comparison between 70 Levels of Met and Met Persisted from Level 59



Area Comparison of Regions with  
Volcanic Ash Air Concentrations  $> 0.2\ g\ m^{-2}$



Comparison between 70 Levels of Met and Met Persisted from Level 59



Area Comparison of Regions with  
Volcanic Ash Air Concentrations  $> 200.0\ \mu g\ m^{-3}$

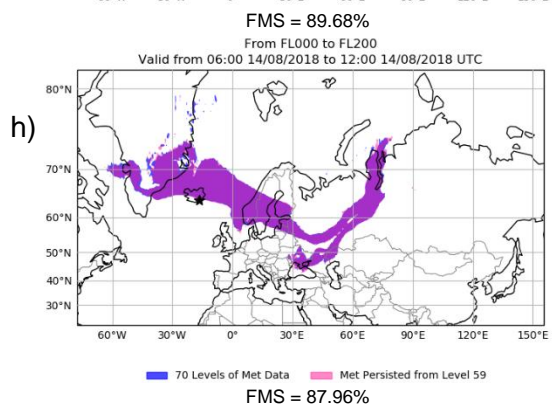
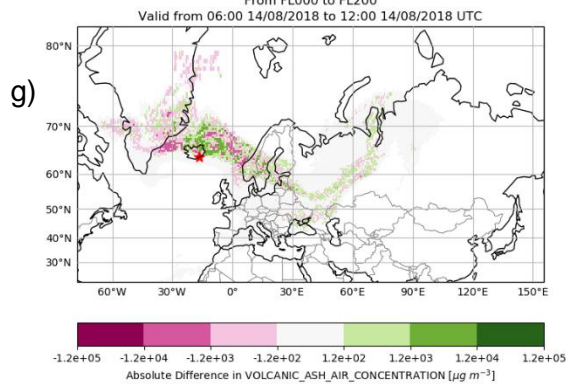
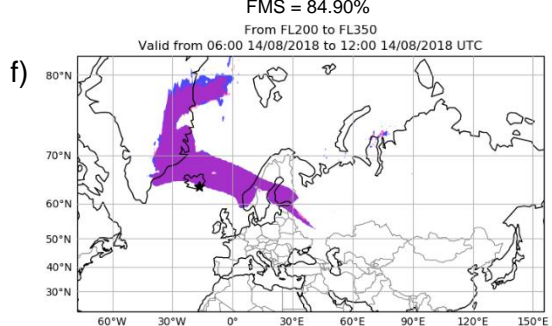
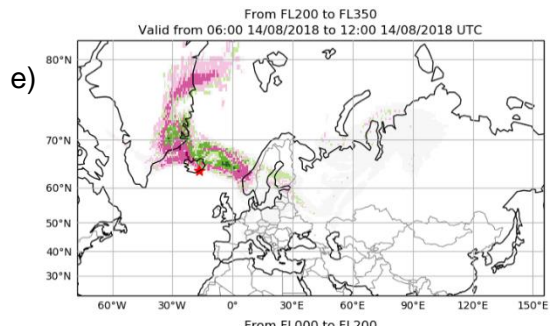
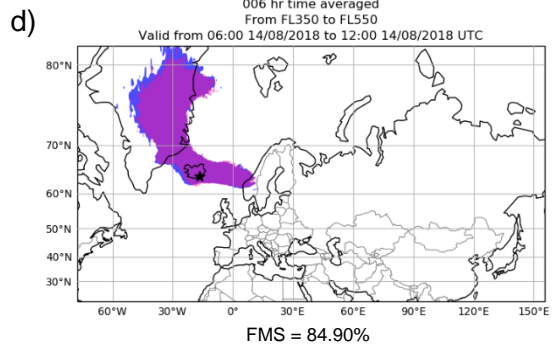


Figure 10: As in Figure 9, but for a release between 30-35 km only, rather than from the summit to 35 km. Note: All flight level layers are below 30 km, the contour scales differ for the total column mass loading and flight level layer differences plots (and differ from Figure 9), and in the area comparison plots the purple region represents an ash cloud area forecast by both met scenarios.

ash cloud area size, due to reduced eastward dispersal at lower levels, and not any particularly large increase in either individual ash cloud area. Compared to the summit to 35 km results, the 30-35 km scenario (Figure 10) shows a reduction in total column FMS of a similar magnitude to that seen in the VI case study, although the flight level areas are not as affected as in the VI event (Figure 3). On the other hand, while the increase in mass loading differences when decreasing the plume depth is similar between the two events, the increase in maximum flight level layer differences is greater for the summer case study period (Table 3).

## 5. Discussion

### 5.1. Overarching Observations from the Case Studies

For the case studies with plumes > 30 km, noticeable differences in the volcanic ash cloud forecasts arose when using the different met datasets. The ash cloud dispersed by Met<sub>70</sub> always spread further perpendicularly to the main dispersion path than the Met<sub>P</sub> cloud as a result of the more varied wind directions present in the non-persisted upper-level met data. Conversely, Met<sub>P</sub> produced ash clouds with higher ash concentration and mass loading biases through the centre of the main dispersion path due to ash particles following the same atmospheric flows at multiple levels.

Large changes in stratospheric wind direction that descend from above will always impose a lag on the Met<sub>P</sub> dispersal conditions, leading to persistent regions of high concentrations of ash heading in the prior direction for longer than they should. This can impact the forecast location of ash at later times as well, with ash potentially being transported from areas where the concentrations are higher than they should be. During periods when there is no major change in stratospheric wind direction, whether ash is dispersed a similar distance when using Met<sub>P</sub> over Met<sub>70</sub> depends on if wind speeds are generally increasing or decreasing with height. If they are increasing with height, such as during post-SSW vortex recovery, pre-VI growth or during more stable winter and summer months, then Met<sub>P</sub> tends to disperse ash less far than using the full Met<sub>70</sub>. If wind speeds are decreasing with height, such as during SSW and FSW onset and post-VI recovery, then ash tends to be dispersed further using the persisted Met<sub>P</sub>. However, the extent to which the dispersal distances differ varies depending on the exact conditions during an event, as seen when comparing the two SSWs.

The extra spreading of ash by Met<sub>70</sub> seen ahead of the 2018 SSW event shows that there are stratospheric phenomena other than those explored here that can also affect the path of simulated ash above 30 km. It also shows that if the resultant differences in ash concentration at upper levels (inferred from the mass loading values) are not of a large enough magnitude, then the differences fail to transfer to the flight level layer forecasts. However, in general, dispersal differences have a greater impact on the areal extent of the ash cloud in the flight level layers when they occur over regions where ash has not already spread to at the lower altitudes. This is made more apparent when looking at the results from the limited depth releases that mimic an umbrella cloud. Here, greater differences are seen in the flight level layers, both as a result of there being no identical dispersal of ash from the source at lower altitudes to form the basis of the lower levels of the ash cloud and because all of the particles are released into altitudes with different met conditions to begin with so even once they reach lower altitudes there will be an increased number of varied dispersal paths affecting the structures of the ash clouds. This shows that, for an umbrella cloud eruptive plume, we might expect the error in forecast ash cloud extents, ash mass loadings and ash concentrations to be larger when using Met<sub>P</sub> over Met<sub>70</sub> than with other plume types.

The two opposing trends in FMS seen during the 2018 SSW event are present throughout the majority of the other study periods as well (Appendix Figure A1). They imply that the choice of met data becomes less important with increasing forecast time when considering the evolution

of the total ash cloud column, but more important when considering the flight level layer forecasts, for plume heights > 30 km. Looking at the limited depth release scenarios shows much the same, although during the VI event the flight level layers' FMS values appear to show some recovery at later times and during the summer period the total column FMS continues to decrease with time. Comparing these trends to each other and those seen in the equivalent summit to 35 km releases shows them to be an exaggeration of the trends seen during the deeper releases and likely not the result of using a shallower release depth given that the apparent changes from the general observed trend are not the same for both events.

The relationship between FMS and maximum ash concentration and ash mass loading differences seen in Figure 4 is the result of less dispersive conditions producing smaller ash clouds with higher central ash concentrations that in turn can produce larger concentration and mass loading differences. That differences of comparable orders of magnitude to the maximum values occur over large areas, as seen in the differences plots, implies that the relationship is not simply the result of random point values skewing the data either. This shows that although using Met<sub>P</sub> during the high FMS case study periods may not have overly affected the size of the forecast ash cloud area where ash concentrations > 200  $\mu\text{g m}^{-3}$  (mass loadings > 0.2  $\text{g m}^{-2}$ ), it still affected the intra-cloud movements of the ash. Therefore, it is possible that the size of the forecast areas for higher contamination thresholds could be affected even if the lowest threshold area is not. Indeed, looking at ash cloud areas and FMS values for thresholds of 2000  $\mu\text{g m}^{-3}$  and 4000  $\mu\text{g m}^{-3}$  (2  $\text{g m}^{-2}$  and 4  $\text{g m}^{-2}$ ) (not shown here) found that although the FMS values did not become smaller for all case studies, the areas where Met<sub>P</sub> exclusively forecast ash above these thresholds were larger for most events. In some cases, however, the large concentration and mass loading differences seen between the two simulated ash clouds occurred in areas within the higher thresholds tested so no greater areal differences were seen.

## **5.2. Limitations of this Study**

Studying these events has highlighted areas which could have been explored further to give more well-rounded results applicable to more situations. The effect that the unexpected meteorological conditions ahead of the 2018 SSW  $U_{10,60}$  reversal had on the ash cloud dispersal and the presence of dispersal differences during the relatively stable summer 2018 period suggest that exploring additional 'normal' conditions for each season would have been beneficial. A broader selection of events would help to identify other less obvious conditions that can affect stratospheric ash dispersal and help to verify the occurrence of dispersal differences under more meteorological circumstances. A simpler method to identify the likely effect that using persisted met data would have on ash dispersion during a wide range of conditions would be to compare the meteorology above 30 km directly and determine typical differences in dispersal characteristics during different seasons and events. In addition, while the two limited depth release scenarios provide good evidence towards there being greater forecast differences between the two met data choices when more of the plume is released into the persisted meteorology, running all of the case studies under such circumstances would have added to this further. Similarly, some of the details of the changing meteorological conditions were lost during the latter parts of the forecast periods due to the clouds becoming

so large. Running shorter simulations over different stages of the events may have made the results easier to interpret. Using other techniques, such as particle trajectories, vertical cross-sections and other statistical analyses, to investigate the internal movements and structural differences of the ash clouds may have helped when analysing the larger clouds as well, along with allowing for a better understanding of how the flight level layer forecasts end up being affected by upper-level differences in dispersal.

### 5.3. Technical Considerations

In order to make a decision on how higher altitude met data should be introduced on the operational system, the technical changes required to implement either option must also be considered:

- Choosing the Met<sub>P</sub> approach would require the fewest changes, with only a simple modification to the flow domain extent within the met definition files. This option would not change the met file names or contents and thus have no impact on other operational systems that share the same met for use with NAME, nor increase the storage requirements or met loading times.
- On the other hand, using Met<sub>70</sub> would increase met generation processing costs to output and convert additional levels of MetUM data into the NAME compatible format, along with increasing the storage requirements for both operational and research purposes. Choosing Met<sub>70</sub> also gives a couple of implementation options:
  - *To store and load all the met data levels into one set of files.*
    - This would require the files to be stored under a new naming convention, which would affect all operational NAME runs using MetUM Global data.
    - This would increase the run times of all operational and research NAME runs using MetUM Global data by approximately 5-10 %, due to the additional met data being loaded regardless of whether the run uses any met data above 30 km.
    - There is an option to have a second met definition file available that would only load the Met<sub>70</sub> data up to the 59<sup>th</sup> level which would lessen the load times for runs that do not require the extra data, but not the additional storage or file name changes needed.
  - *To split the met data into two sets of height ranges.*
    - This gives the option to only store met data above 30 km long term when an event that requires it occurs, lessening the increased storage requirements. Though this may be difficult to implement in practice.
    - Assuming that the split in data occurs at the 59<sup>th</sup> level, there would be no need to make any changes to other associated NAME systems that only use MetUM Global data at lower altitudes and the run times for these systems would remain the same.
    - There is the option to split the met data at a lower altitude, which would require changes to all associated systems but would potentially decrease the run times for events that occur below the new altitude limit.

- Implementing this method would be more work with the need to process the met data into more files than at present and to alter the met definition files to read in multiple level range files.
- Should the decision to use a height other than 30 km be made, additional work would need to be completed to determine the best cut-off height for the lower-level data.

Future changes in NWP resolution (both horizontal and vertical) and storage format should also be considered when thinking about the pros and cons of each option as this will potentially change the significance of any storage volume increases associated with adding extra levels and influence the decision to split data across multiple files. For example, it may be decided that adding an upper-level height cap greater than 30 km but less than the top of the MetUM Global domain (currently 80 km) is beneficial in limiting excessive storage and reading in of unnecessary met data given the likelihood of volcanic ash or other particulates reaching such altitudes.

## 6. Conclusions

- The 1875 AD eruption of Askja volcano is the last known event in Iceland to have generated a plume estimated to reach an altitude  $\geq 30$  km, while the most recent global VEI 5, 6 and 7 events are the 2011 Puyehue-Cordón Caulle eruption (~12 km plume height), the 1991 Pinatubo eruption (30-35 km plume height) and the 1815 Tambora eruption (~43 km plume height), respectively (Sigurdsson and Carey 1989, Global Volcanism Program 2013). This demonstrates that eruptions above 30 km are possible and should be planned for.
- Stratospheric meteorological events that could affect ash dispersion occur as frequently as annually or biennially.
- This work has investigated the impact of using persisted meteorology above 30 km (Met<sub>P</sub>) versus full NWP met data (Met<sub>70</sub>) when modelling the transport and dispersion of stratospheric volcanic ash.
- When simulating the dispersal of ash from plumes  $< 30$  km in height, there are no significant differences in the ash clouds produced by the two met options.
- When simulating plumes  $> 30$  km, using Met<sub>70</sub> transports and disperses ash more broadly, while the ash clouds simulated using Met<sub>P</sub> appear narrower with higher ash mass loadings in the centre of the clouds. The subsequent effect on the concentration of ash in individual flight level layers is similar, but the differences are less distinct at lower altitudes.
- Events with significant shifts in stratospheric zonal wind direction or speed that have a height dependency lead to the largest differences in ash cloud extent when comparing the two met set-ups.
- During events where using Met<sub>P</sub> has little influence on the horizontal extent of the simulated ash cloud, the central ash mass loading and concentration differences become large because the differences in dispersal and the total ash volume are confined to a smaller area. This can then influence the size of higher threshold forecast areas.
- Even when there is no distinct stratospheric meteorological event occurring (e.g. during summer) differences in the predicted transport and dispersion of the ash cloud occur when using Met<sub>P</sub>. Additionally, unexpected/unexplained stratospheric conditions can have an effect as well (e.g. the plume streak during the 2018 SSW).
- The differences in the spread of the simulated ash clouds in the flight level layers are greatest when the stratospheric dispersal of ash is in the opposite direction to the tropospheric dispersal or when no ash is released at tropospheric levels (e.g. with an umbrella cloud) as the ash settling from above is then not concealed by pre-existing areas of ash. Flight level layer ash cloud differences, in both area and concentration, are also greater in locations where the mass loading differences are larger.
- Differences in the forecast ash mass loading and concentration values are greatest when all of the ash is released over a limited depth at altitudes  $> 30$  km, representative of an umbrella cloud.

- Based on the evidence presented here, it is recommended that all available NWP met data covering the altitudes volcanic ash is likely to reach (not necessarily Met<sub>70</sub>) should be used in order to best represent the transport and dispersion of ash at altitudes > 30 km when generating volcanic ash forecasts.

## **7. Acknowledgements**

This work builds on the PhD project by Jennifer Saxby. The authors would also like to acknowledge the support of Claire Witham and Susan Leadbetter, without which the project would not have been instigated, Helen Webster for assistance with troubleshooting NAME, Benjamin Evans for help with figure production, and Andrew Bushell for scientific guidance.



## References

- Barsotti, S., D. I. Di Rienzo, T. Thordarson, B. B. Björnsson, and S. Karlsdóttir, 2018: Assessing Impact to Infrastructures Due to Tephra Fallout From Öræfajökull Volcano (Iceland) by Using a Scenario-Based Approach and a Numerical Model. *Front. Earth Sci.* **6**, 196, <https://doi.org/10.3389/feart.2018.00196>.
- Beckett, F. M., C. S. Witham, S. J. Leadbetter, R. Crocker, H. N. Webster, M. C. Hort, A. R. Jones, B. J. Devenish, and D. J. Thomson, 2020: Atmospheric Dispersion Modelling at the London VAAC: A Review of Developments since the 2010 Eyjafjallajökull Volcano Ash Cloud. *Atmosphere*, **11**, 352, <https://doi.org/10.3390/atmos11040352>.
- Berrisford, P., D. P. Dee, K. Fielding, M. Fuentes, P. Kållberg, S. Kobayashi, S. M. Uppala, 2009: The ERA-Interim Archive. ERA Report Series No. 1, 16 pp, <https://www.ecmwf.int/sites/default/files/elibrary/2009/8173-era-interim-archive.pdf>.
- Black, R. X., and B. A. McDaniel, 2007: The Dynamics of Northern Hemisphere Stratospheric Final Warming Events. *J. Atmos. Sci.*, **64**, Issue 8, 2932–2946, <https://doi.org/10.1175/JAS3981.1>.
- Butler, A. H., J. P. Sjöberg, D. J. Seidel, and K. H. Rosenlof, 2017: A sudden stratospheric warming compendium, *Earth Syst. Sci. Data*, **9**, 63–76, <https://doi.org/10.5194/essd-9-63-2017>.
- Butler, A. H., Z. D. Lawrence, S. H. Lee, S. P. Lillo, C. S. Long, 2020: Differences between the 2018 and 2019 stratospheric polar vortex split events. *Quart. J. Roy. Meteor. Soc.*, **146**, 3503– 3521. <https://doi.org/10.1002/qj.3858>
- CAA, 2017: Guidance regarding flight operations in the vicinity of volcanic ash Version 2. CAP1236, 33 pp, <https://publicapps.caa.co.uk/docs/33/CAP%201236%20FEB17.pdf>.
- Carey, R. J., B. F. Houghton, and T. Thordarson, 2010: Tephra dispersal and eruption dynamics of wet and dry phases of the 1875 eruption of Askja Volcano, Iceland. *Bull. Volcanol.*, **72**, 259–278, <https://doi.org/10.1007/s00445-009-0317-3>.
- Casadevall, T. J., 1994: The 1989–1990 eruption of Redoubt Volcano, Alaska: impacts on aircraft operations. *J. Volcanol. Geotherm. Res.*, **62**, Issues 1–4, 301–316, [https://doi.org/10.1016/0377-0273\(94\)90038-8](https://doi.org/10.1016/0377-0273(94)90038-8).
- Casadevall, T. J., P. J. Delos Reyes, and D. J. Schneider, 1996: The 1991 Pinatubo eruptions and their effects on aircraft operations. *Fire and Mud: Eruptions and Lahars of Mount Pinatubo, Philippines*, Newhall, C.G., and R. S. Punongbayan, Eds., University of Washington Press, and PHILVOCS, 625–636.
- Charlton, A. J., and L. M. Polvani, 2007: A New Look at Stratospheric Sudden Warmings. Part I: Climatology and Modeling Benchmarks, *J. Climate*, **20**, Issue 3, 449–469, <https://doi.org/10.1175/JCLI3996.1>.
- Craig, R. A., 1965: *The Upper Atmosphere Meteorology and Physics*. Academic Press, 509 pp.

Devenish, B. J., 2013: Using simple plume models to refine the source mass flux of volcanic eruptions according to atmospheric conditions. *J. Volcanol. Geotherm. Res.*, **256**, 118-127, <https://doi.org/10.1016/j.jvolgeores.2013.02.015>.

Global Volcanism Program, 2013: Volcanoes of the World, v. 4.10.1 (29 Jun 2021). Venzke, E (ed.), Smithsonian Institution, accessed 16 Aug 2021. <https://doi.org/10.5479/si.GVP.VOTW4-2013>.

Greening, K. and A. Hodgson, 2019: Atmospheric analysis of the cold late February and early March 2018 over the UK. *Weather*, **74**, 79-85, <https://doi.org/10.1002/wea.3467>.

Hare, F. K., 1960: The summer circulation of the arctic stratosphere below 30 km. *Quart. J. Roy. Meteor. Soc.*, **86**, 127-143, <https://doi.org/10.1002/qj.49708636802>.

Hurrell, J. W., Y. Kushnir, G. Ottersen, and M. Visbeck, 2003: An overview of the North Atlantic Oscillation. *The North Atlantic Oscillation: Climate Significance and Environmental Impact*, *Geophys. Monogr.*, Vol. 134, Amer. Geophys. Union, 1-35, <https://doi.org/10.1029/134GM01>.

Hurrell, J. W., Y. Kushnir, M. Visbeck, 2001: The North Atlantic Oscillation., *Science*, **291**, Issue 5504, 603-605, <https://doi.org/10.1126/science.1058761>.

ICAO, 2021: Volcanic Ash Contingency Plan – European and North Atlantic Regions (EUR/NAT VACP, EUR Doc 019, NAT Doc 006 Part II) – Edition 2.0.1., 75 pp, <https://www.icao.int/EURNAT/EUR%20and%20NAT%20Documents/EUR+NAT%20VACP%20v2.0.1.pdf>.

IPCC, 2007: Climate Change 2007 - The Physical Science Basis: Working Group I Contribution to the Fourth Assessment Report of the Intergovernmental Panel on Climate Change, Solomon S., D. Qin, M. Manning, Z. Chen, M. Marquis, K. B. Averyt, M. Tignor, H. L. Miller, Eds., Cambridge Univ. Press, 996 pp.

Jones, A. R., D. J. Thomson, M. Hort, and B. Devenish, 2007: The U.K. Met Office's next-generation atmospheric dispersion model, NAME III. *Air Pollution Modeling and its Application XVII*, Borrego, C., and Norman, A.L., Eds., Springer, 580–589, [https://doi.org/10.1007/978-0-387-68854-1\\_62](https://doi.org/10.1007/978-0-387-68854-1_62).

Karpechko, A. Y., A. Charlton-Perez, M. Balmaseda, N. Tyrrell, and F. Vitart, 2018: Predicting sudden stratospheric warming 2018 and its climate impacts with a multimodel ensemble. *Geophys. Res. Lett.*, **45**, 13,538-13,546. <https://doi.org/10.1029/2018GL081091>.

Kiyosugi, K., C. Connor, R. S. J. Sparks, H. S. Crosweller, S. K. Brown, L. Siebert, T. Wang, and S. Takarada, 2015: How many explosive eruptions are missing from the geologic record? Analysis of the quaternary record of large magnitude explosive eruptions in Japan. *J. Appl. Volcanol.*, **4**, 17, <https://doi.org/10.1186/s13617-015-0035-9>.

Lacasse, C., 2001: Influence of climate variability on the atmospheric transport of Icelandic tephra in the subpolar North Atlantic. *Global Planet. Change*, **29**, Issues 1-2, 31-35, [https://doi.org/10.1016/S0921-8181\(01\)00099-6](https://doi.org/10.1016/S0921-8181(01)00099-6).

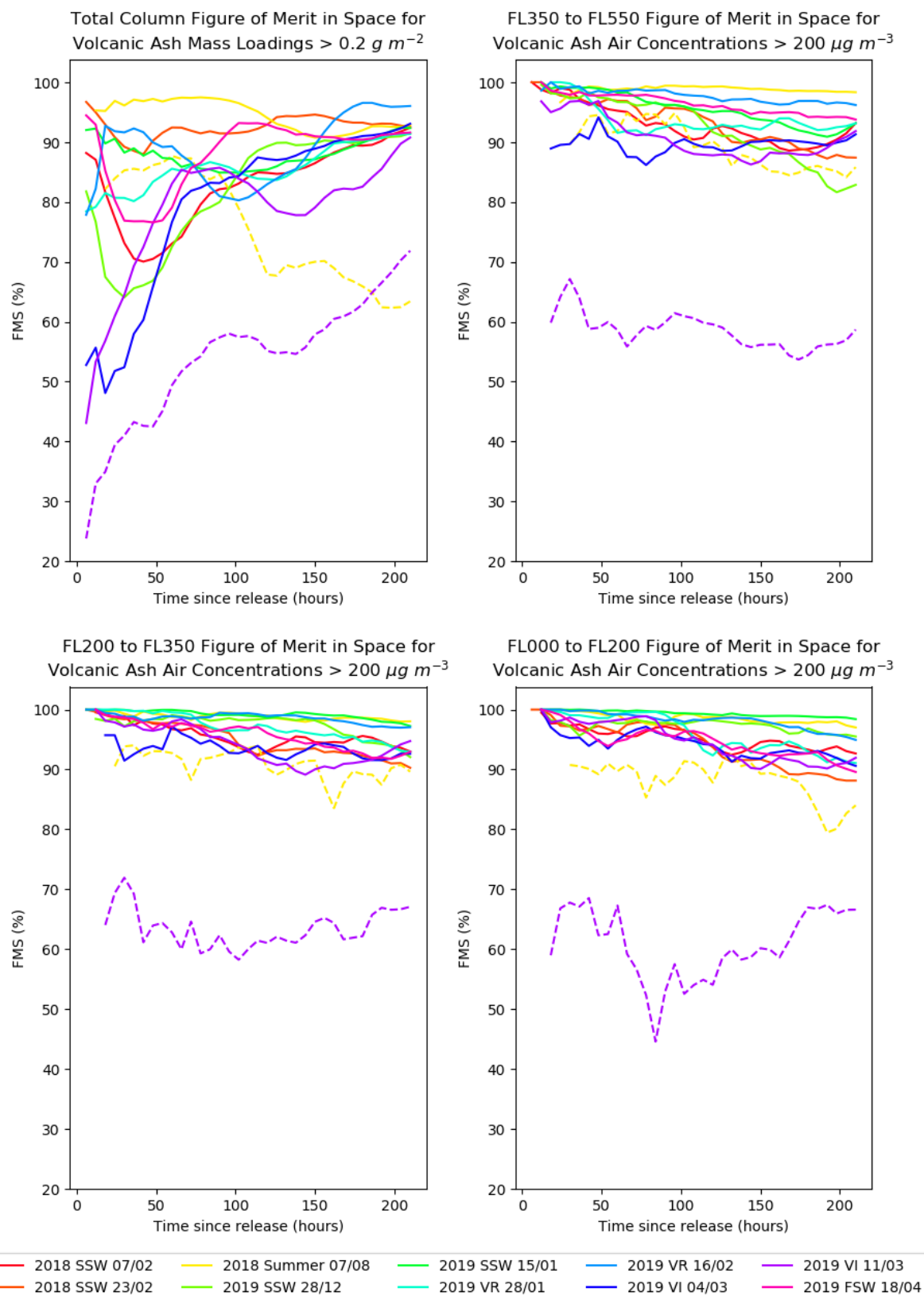
- Leadbetter, S. J., and M. C. Hort, 2011: Volcanic ash hazard climatology for an eruption of Hekla Volcano, Iceland. *J. Volcanol. Geotherm. Res.*, **199**, Issues 3-4, 230-241, <https://doi.org/10.1016/j.jvolgeores.2010.11.016>.
- Lee, S. H., and A. H. Butler, 2020: The 2018–2019 Arctic stratospheric polar vortex. *Weather*, **75**, 52-57, <https://doi.org/10.1002/wea.3643>.
- Limpasuvan, V., D. L. Hartmann, D. W. J. Thompson, K. Jeev, and Y. L. Yung, 2005: Stratosphere-troposphere evolution during polar vortex intensification, *J. Geophys. Res.*, **110**, D24101, <https://doi.org/10.1029/2005JD006302>.
- Limpasuvan, V., D. W. J. Thompson, and D. L. Hartmann, 2004: The Life Cycle of the Northern Hemisphere Sudden Stratospheric Warmings. *J. Climate*, **17**, Issue 13, 2584-2596, [https://doi.org/10.1175/1520-0442\(2004\)017%3C2584:TLCOTN%3E2.0.CO;2](https://doi.org/10.1175/1520-0442(2004)017%3C2584:TLCOTN%3E2.0.CO;2).
- Mastin, L. G., M. Guffanti, R. Servranckx, P. Webley, S. Barsotti, K. Dean, A. Durant, J. W. Ewert, A. Neri, W. I. Rose, D. Schneider, L. Siebert, B. Stunder, G. Swanson, A. Tupper, A. Volentik, C. F. Waythomas, 2009: A multidisciplinary effort to assign realistic source parameters to models of volcanic ash-cloud transport and dispersion during eruptions. *J. Volcanol. Geotherm. Res.*, **186**, Issues 1-2, 10-21, <https://doi.org/10.1016/j.jvolgeores.2009.01.008>.
- Newhall C., S. Self, and A. Robock, 2018: Anticipating future Volcanic Explosivity Index (VEI) 7 eruptions and their chilling impacts. *Geosphere*, **14**, Issue 2, 572-603, <https://doi.org/10.1130/GES01513.1>.
- Newhall, C. G., and S. Self, 1982: The volcanic explosivity index (VEI) an estimate of explosive magnitude for historical volcanism. *J. Geophys. Res.*, **87**, Issue C2, 1231– 1238, <https://doi.org/10.1029/JC087iC02p01231>.
- Oxford Economics, 2010: The economic impacts of air travel restrictions due to volcanic ash: 15 pp, <https://www.oxfordeconomics.com/my-oxford/projects/129051>.
- Saxby, J., A. Rust, K. Cashman, and F. Beckett, 2020: The importance of grain size and shape in controlling the dispersion of the Vedde cryptotephra. *J. Quaternary Sci.*, **35**, 175-185, <https://doi.org/10.1002/jqs.3152>.
- Sigurdsson, H., S. Carey, 1989: Plinian and co-ignimbrite tephra fall from the 1815 eruption of Tambora volcano. *Bull. Volcanol.*, **51**, 243-270, <https://doi.org/10.1007/BF01073515>
- Simkin, T., 1993: Terrestrial Volcanism in Space and Time. *Annu. Rev. Earth Planet. Sci.*, **21**, 427-452, <https://doi.org/10.1146/annurev.ea.21.050193.002235>.
- Sparks, R. S. J., 1986: The dimensions and dynamics of volcanic eruption columns. *Bull. Volcanol.*, **48**, 3–15, <https://doi.org/10.1007/BF01073509>.
- Trigo, R. M., T. J. Osborn, J. M. Corte-Real, 2002: The North Atlantic Oscillation influence on Europe: climate impacts and associated physical mechanisms. *Climate Res.*, **20**, 9-17, <https://doi.org/10.3354/cr020009>.
- Tupper, A., C. Textor, M. Herzog, H. Graf, M. S. Richards, 2009: Tall clouds from small

eruptions: the sensitivity of eruption height and fine ash content to tropospheric instability. *Nat. Hazards*, **51**, 375–401, <https://doi.org/10.1007/s11069-009-9433-9>.

Webster, H. N., B. J. Devenish, L. G. Mastin, D. J. Thomson, A. R. Van Eaton, 2020: Operational modelling of umbrella cloud growth in a Lagrangian volcanic ash transport and dispersion model. *Atmosphere*, **11**, 200, <https://doi.org/10.3390/atmos11020200>.

Witham, C., M. Hort, D. Thomson, S. Leadbetter, B. Devenish, H. Webster, F. Beckett, N. Kristiansen, 2021: The current volcanic ash modelling setup at the London VAAC. Met Office Tech. Summary v1.7, 12 pp, <https://library.metoffice.gov.uk/Portal/DownloadImageFile.ashx?fieldValueId=3221>.

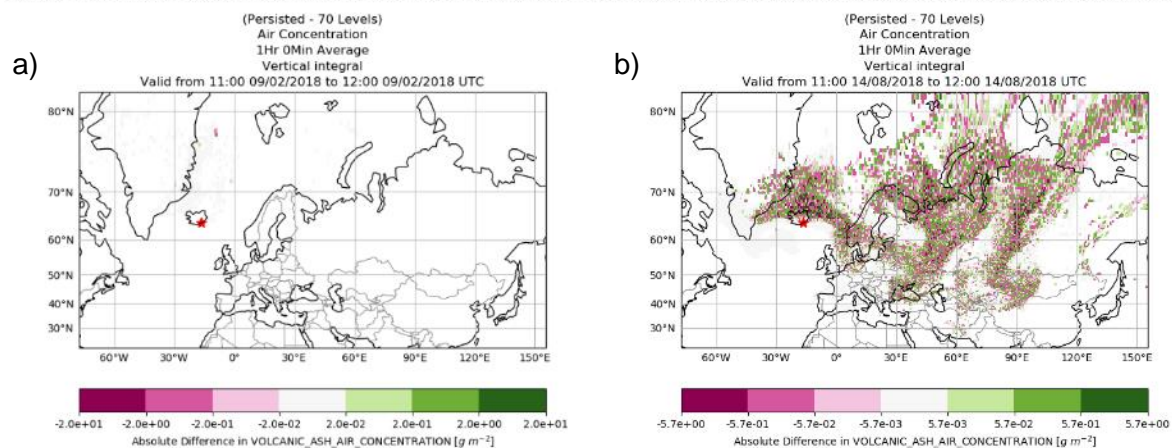
## Appendix



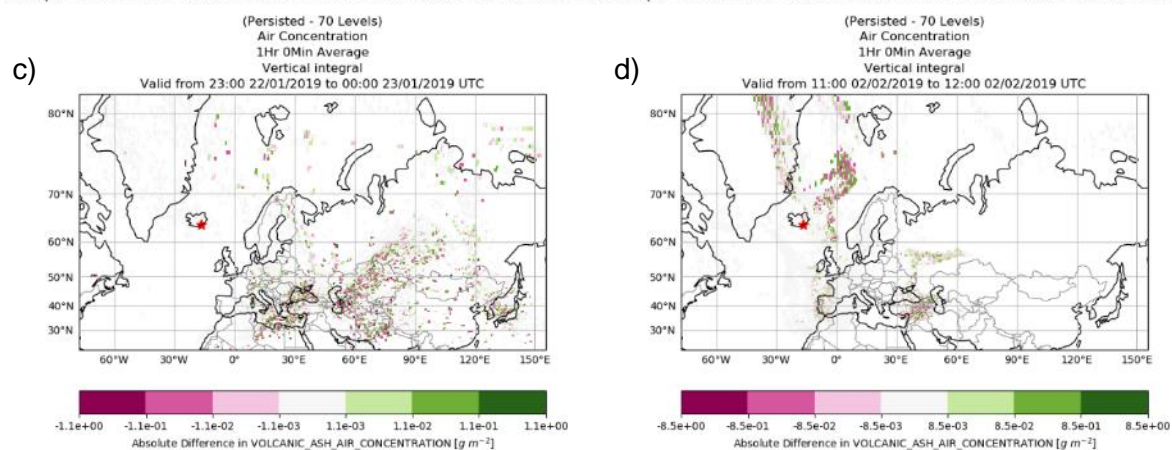
Appendix Figure A1: The evolution of total column and flight level layer FMS values for each 35 km plume case study. Dashed line shows the same for the 30-35 km releases.



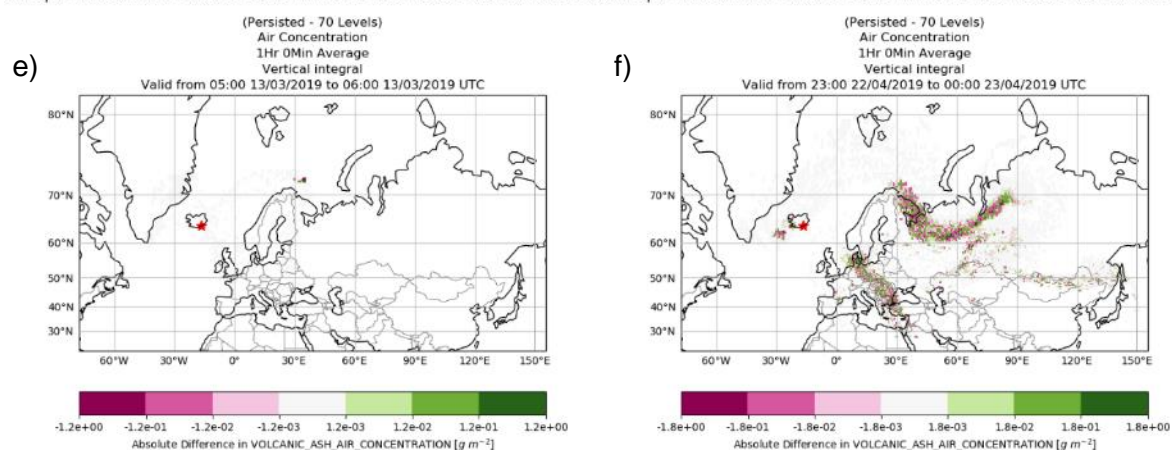
Comparison between 70 Levels of Met and Met Persisted from Level 59 Comparison between 70 Levels of Met and Met Persisted from Level 59



Comparison between 70 Levels of Met and Met Persisted from Level 59 Comparison between 70 Levels of Met and Met Persisted from Level 59

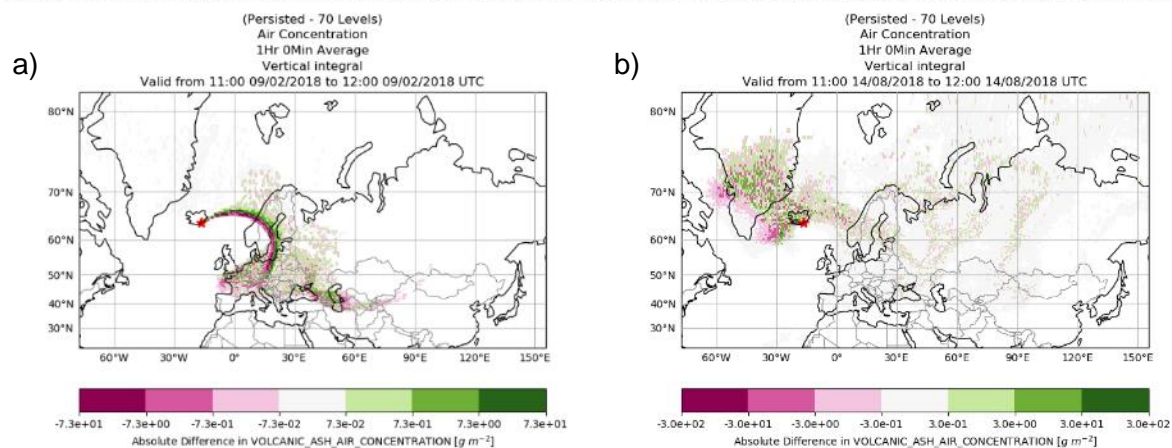


Comparison between 70 Levels of Met and Met Persisted from Level 59 Comparison between 70 Levels of Met and Met Persisted from Level 59

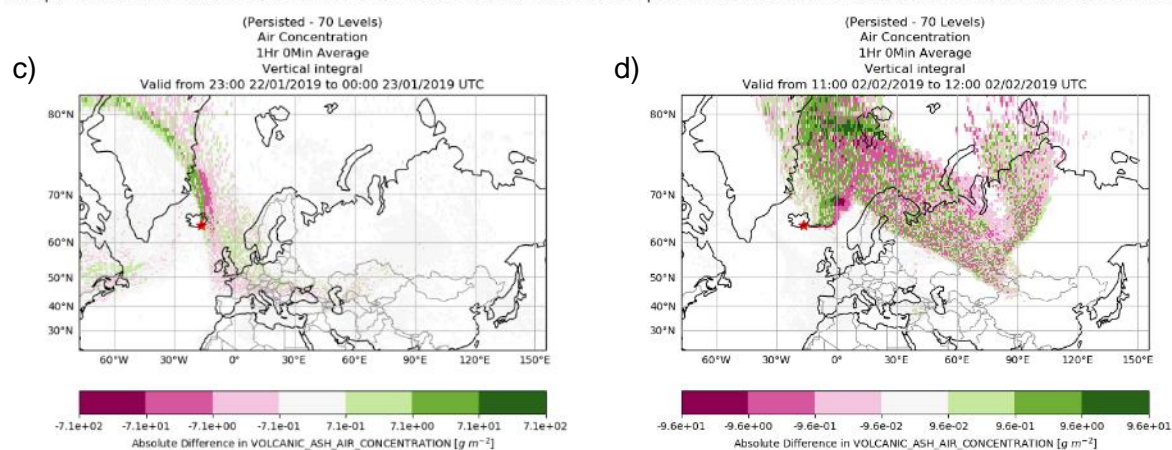


Appendix Figure A2: Total column mass loading differences for 25 km plume simulations for (a) 2018 SSW 07/02 at T+54 (12:00 09/02/2018), (b) 2018 Summer 07/08 at T+174 (12:00 14/08/2018), (c) 2019 SSW 15/01 at T+186 (00:00 23/01/2019), (c) 2019 VR 28/01 at T+126 (12:00 02/02/2019), (d) 2019 VI 11/03 at T+48 (06:00 13/03/2019) and (e) 2019 FSW 18/04 at T+114 (00:00 23/04/2019). Note: The contour scales differ for each case study.

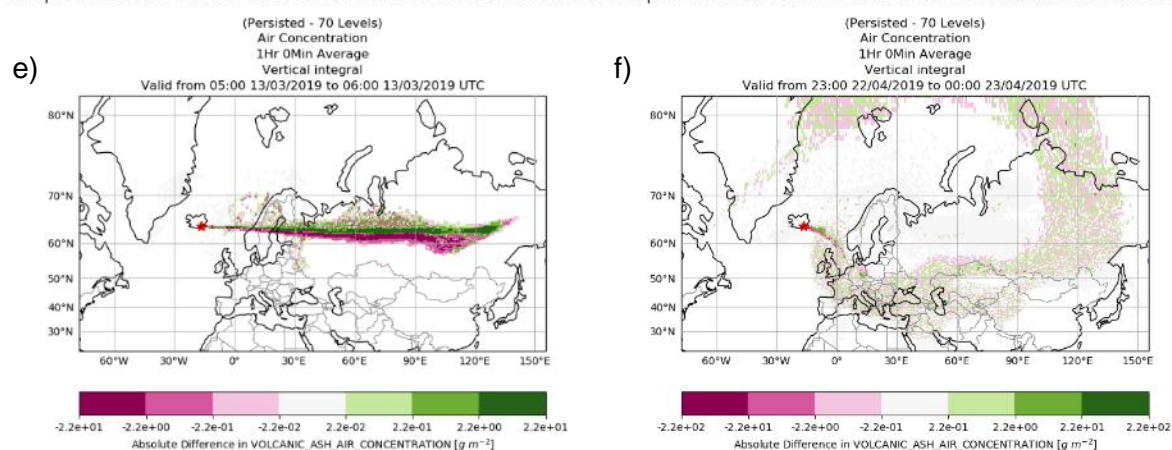
Comparison between 70 Levels of Met and Met Persisted from Level 59 Comparison between 70 Levels of Met and Met Persisted from Level 59



Comparison between 70 Levels of Met and Met Persisted from Level 59 Comparison between 70 Levels of Met and Met Persisted from Level 59



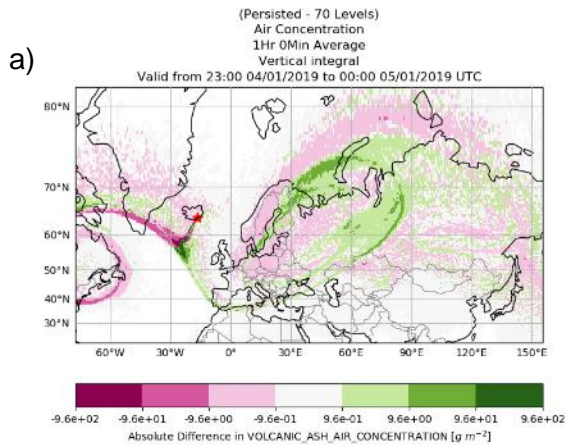
Comparison between 70 Levels of Met and Met Persisted from Level 59 Comparison between 70 Levels of Met and Met Persisted from Level 59



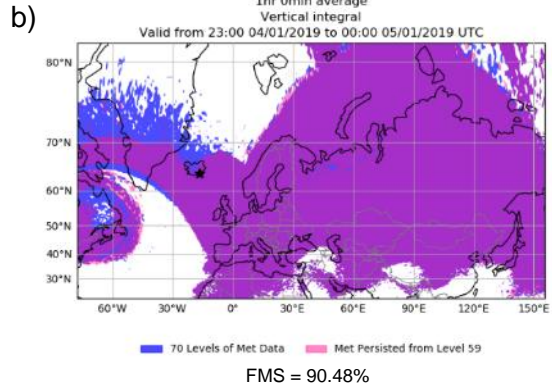
Appendix Figure A3: As in Appendix Figure A2, but for 30 km plume height simulations. Note: The contour scales differ from those in Appendix Figure A2.



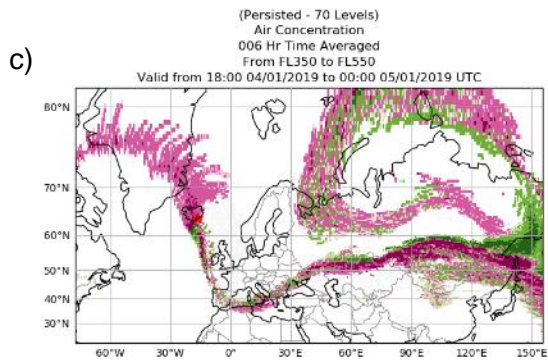
Comparison between 70 Levels of Met and Met Persisted from Level 59



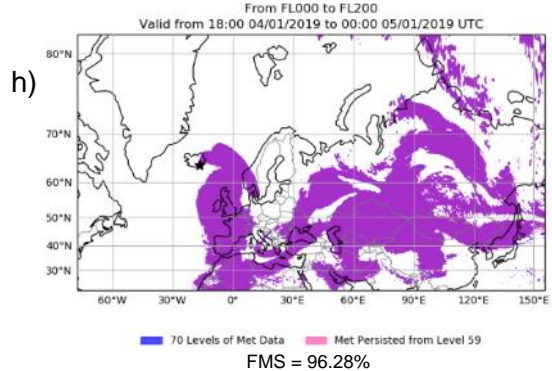
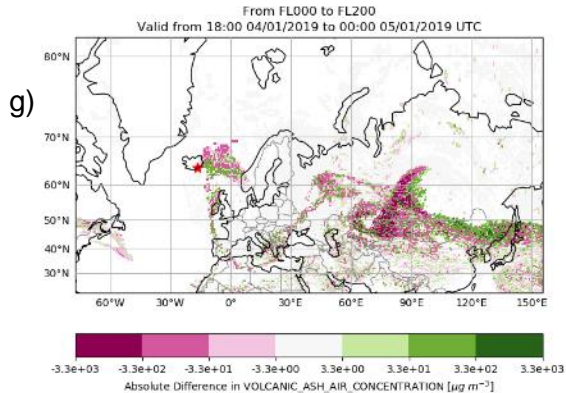
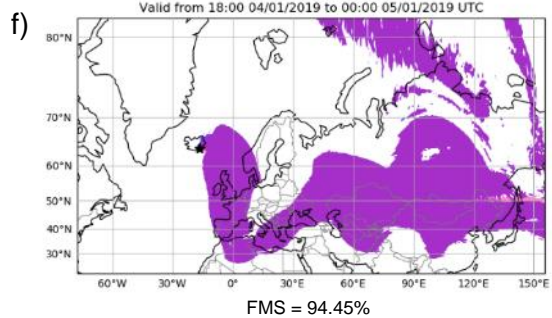
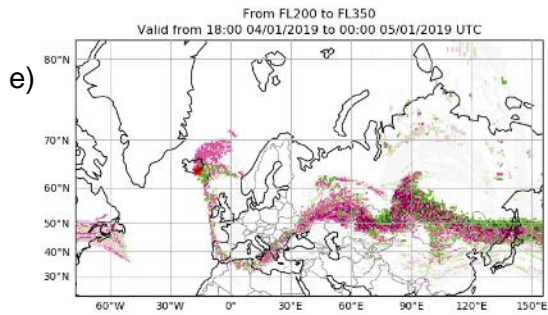
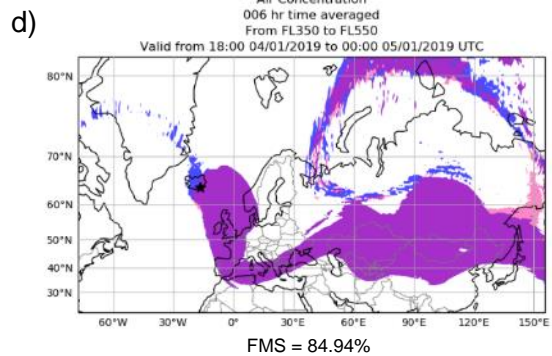
Area Comparison of Regions with  
Volcanic Ash Air Concentrations  $> 0.2\ g\ m^{-2}$



Comparison between 70 Levels of Met and Met Persisted from Level 59



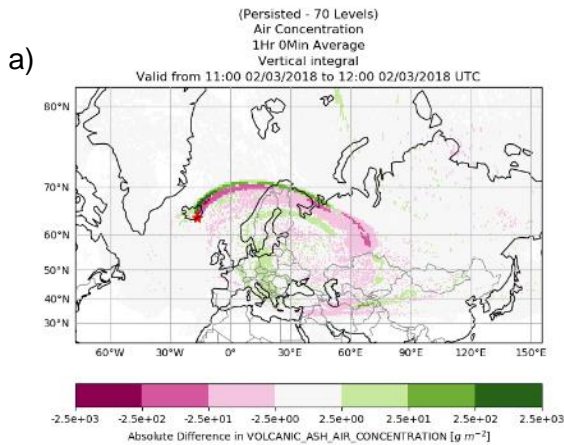
Area Comparison of Regions with  
Volcanic Ash Air Concentrations  $> 200.0\ \mu g\ m^{-3}$



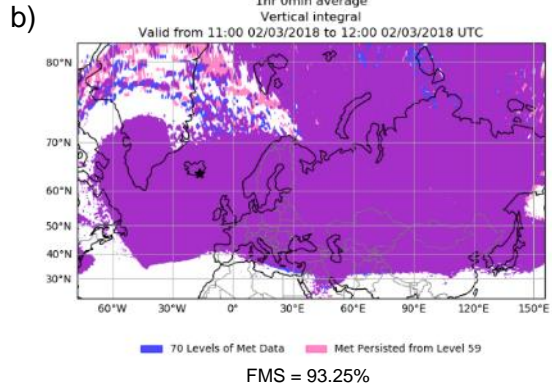
Appendix Figure A4: To compare simulated ash clouds produced using Met<sub>P</sub> and Met<sub>70</sub> during the 2019 SSW 28/12 run at T+186 (00:00 05/01/2019) for a plume height of 35 km. (a) Total column mass loading differences, (b) ash cloud area comparison for mass loading values above  $0.2\ g\ m^{-2}$ , (c, e, g) flight level layer concentration differences and (d, f, h) ash cloud area comparison for concentrations above  $200\ \mu g\ m^{-3}$ . Note: All flight level layers are below 30 km, the contour scales differ for the total column mass loading and flight level layer differences plots, and in the area comparison plots the purple region represents an ash cloud area forecast by both met scenarios.



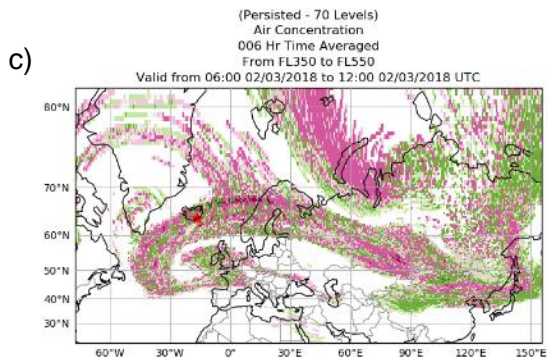
Comparison between 70 Levels of Met and Met Persisted from Level 59



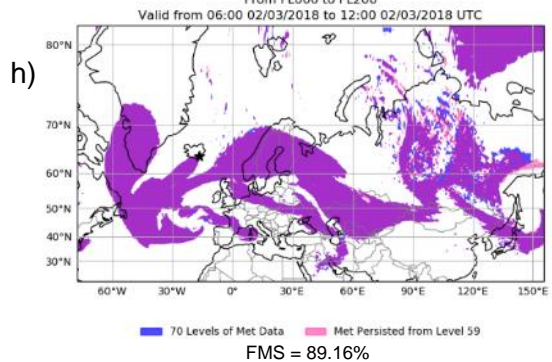
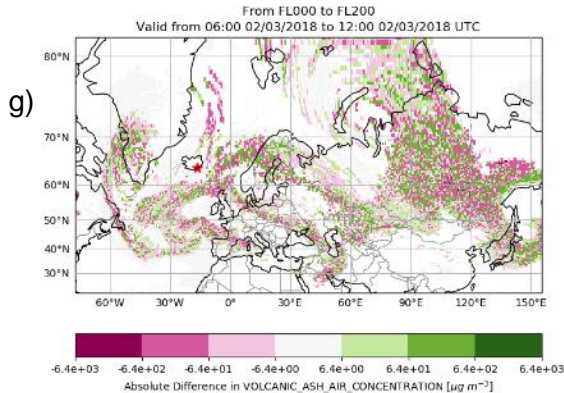
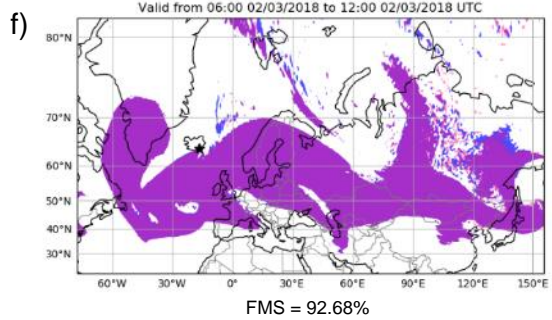
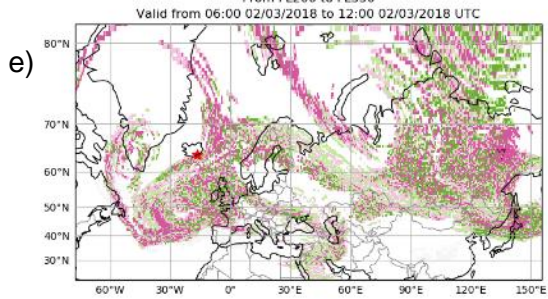
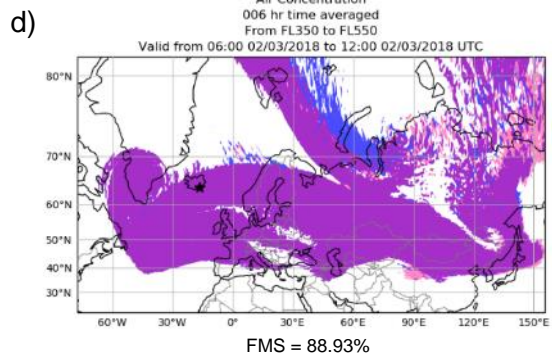
Area Comparison of Regions with  
Volcanic Ash Air Concentrations  $> 0.2\ g\ m^{-2}$



Comparison between 70 Levels of Met and Met Persisted from Level 59



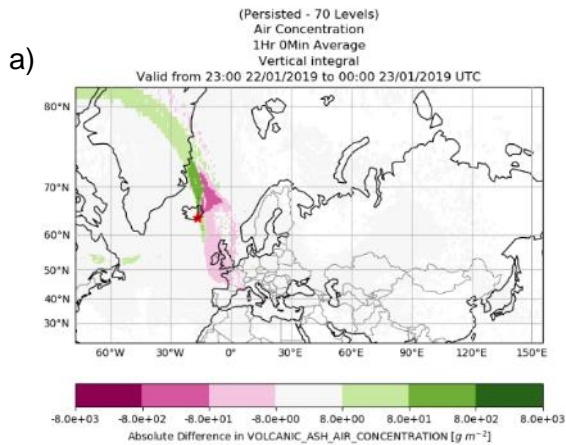
Area Comparison of Regions with  
Volcanic Ash Air Concentrations  $> 200.0\ \mu g\ m^{-3}$



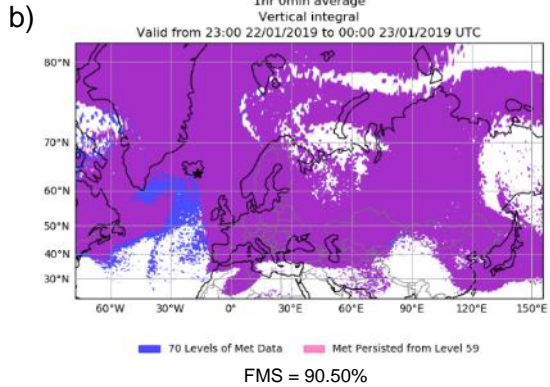
Appendix Figure A5: To compare simulated ash clouds produced using Met<sub>P</sub> and Met<sub>70</sub> during the 2018 SSW 23/02 run at T+174 (12:00 02/03/2018) for a plume height of 35 km. (a) Total column mass loading differences, (b) ash cloud area comparison for mass loading values above  $0.2\ g\ m^{-2}$ , (c, e, g) flight level layer concentration differences and (d, f, h) ash cloud area comparison for concentrations above  $200\ \mu g\ m^{-3}$ . Note: All flight level layers are below 30 km, the contour scales differ for the total column mass loading and flight level layer differences plots, and in the area comparison plots the purple region represents an ash cloud area forecast by both met scenarios.



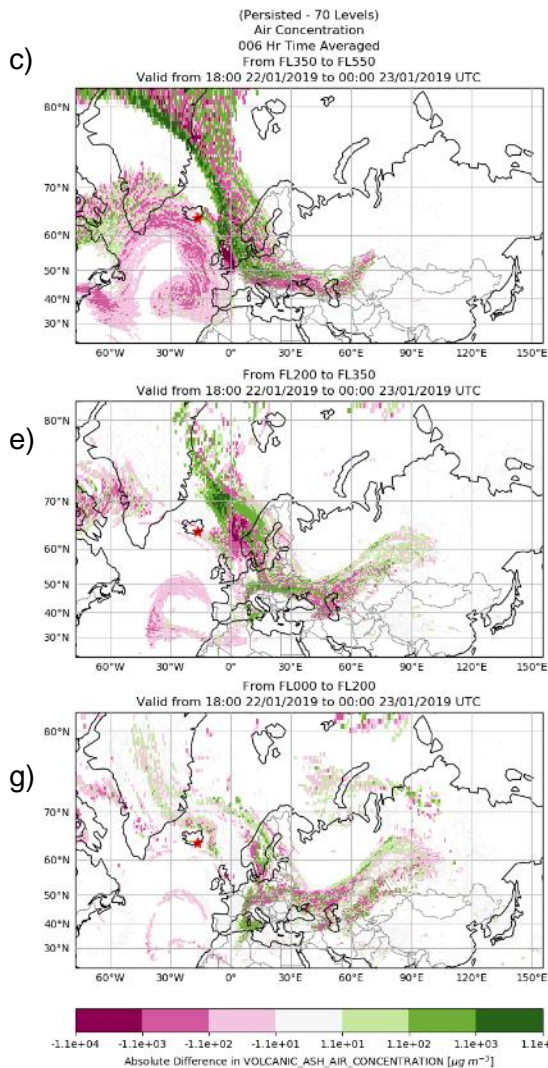
Comparison between 70 Levels of Met and Met Persisted from Level 59



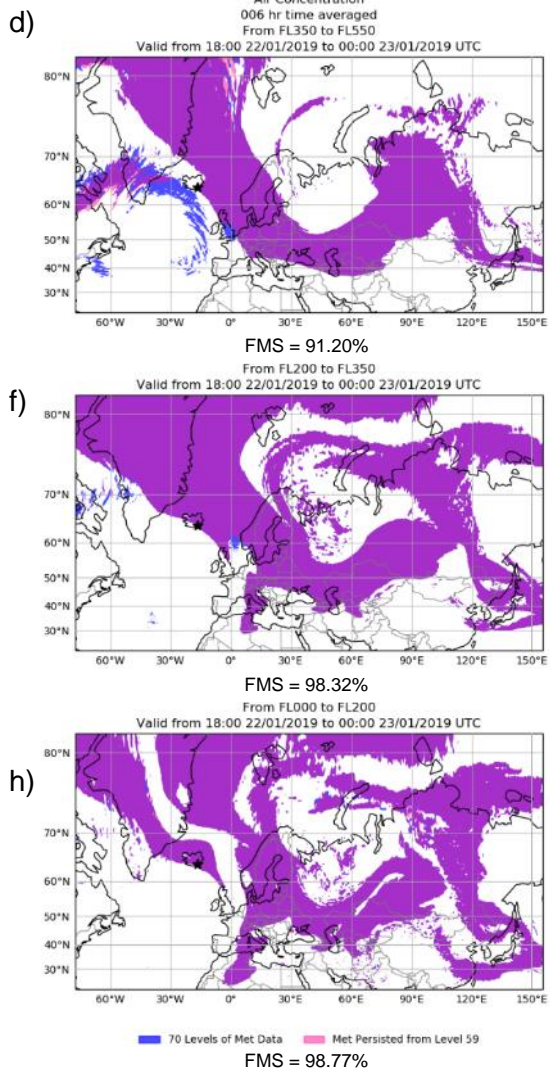
Area Comparison of Regions with  
Volcanic Ash Air Concentrations  $> 0.2 \text{ g m}^{-2}$



Comparison between 70 Levels of Met and Met Persisted from Level 59

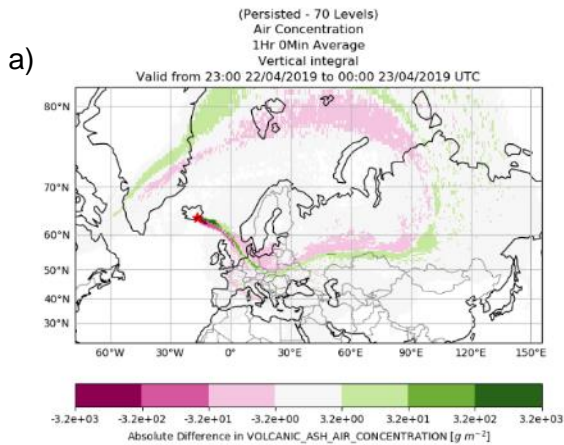


Area Comparison of Regions with  
Volcanic Ash Air Concentrations  $> 200.0 \mu\text{g m}^{-3}$

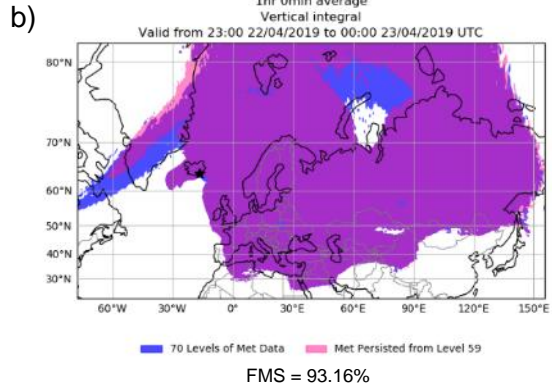


Appendix Figure A6: To compare simulated ash clouds produced using Met<sub>p</sub> and Met<sub>70</sub> during the 2019 SSW 15/01 run at T+186 (00:00 23/01/2019) for a plume height of 35 km. (a) Total column mass loading differences, (b) ash cloud area comparison for mass loading values above  $0.2 \text{ g m}^{-2}$ , (c, e, g) flight level layer concentration differences and (d, f, h) ash cloud area comparison for concentrations above  $200 \mu\text{g m}^{-3}$ . Note: All flight level layers are below 30 km, the contour scales differ for the total column mass loading and flight level layer differences plots, and in the area comparison plots the purple region represents an ash cloud area forecast by both met scenarios.

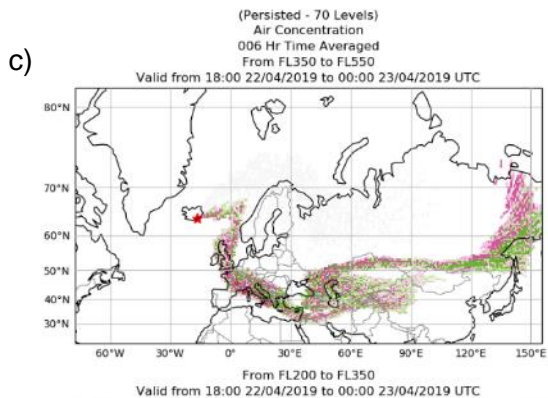
Comparison between 70 Levels of Met and Met Persisted from Level 59



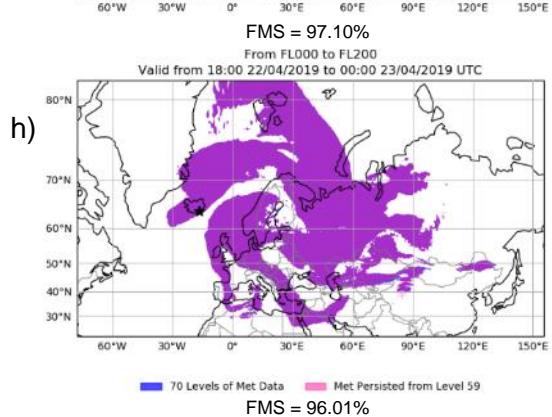
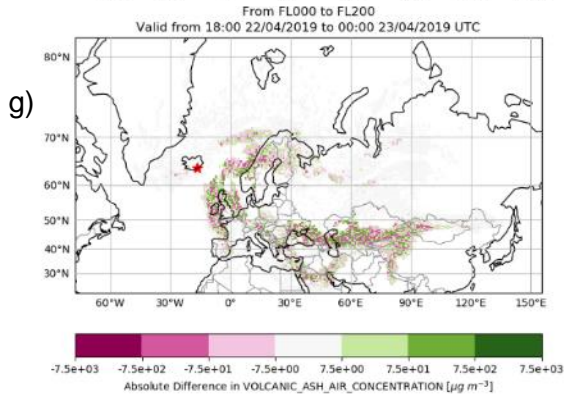
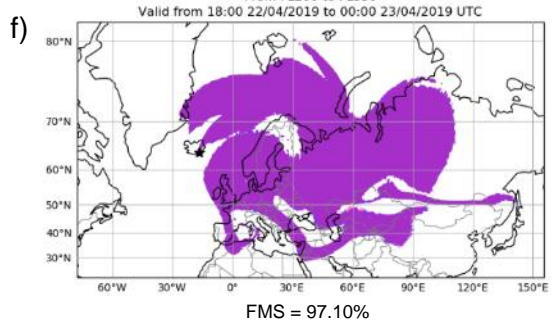
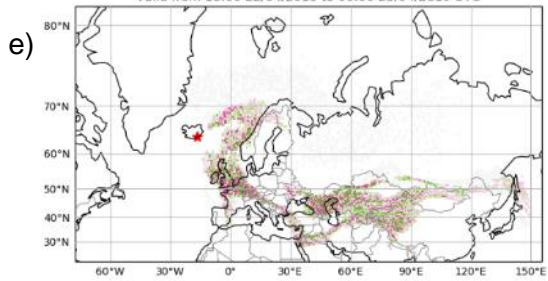
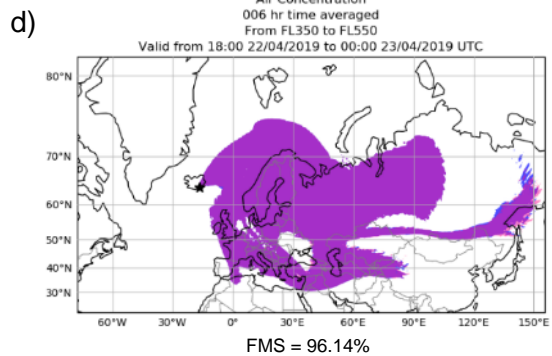
Area Comparison of Regions with  
Volcanic Ash Air Concentrations  $> 0.2 \text{ g m}^{-2}$



Comparison between 70 Levels of Met and Met Persisted from Level 59



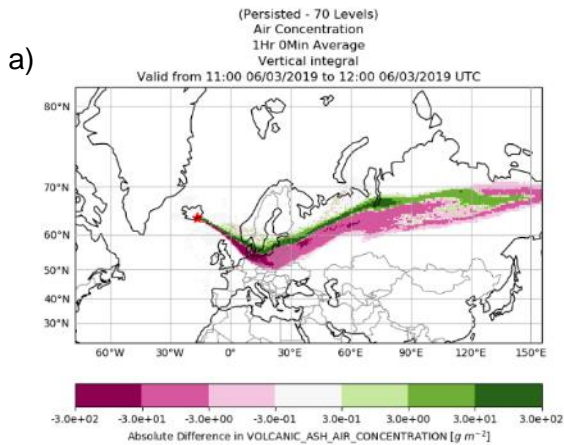
Area Comparison of Regions with  
Volcanic Ash Air Concentrations  $> 200.0 \mu\text{g m}^{-3}$



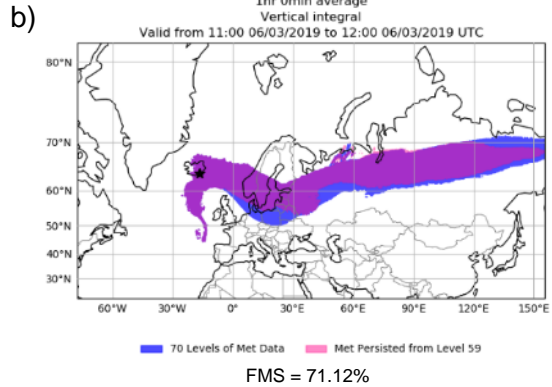
Appendix Figure A7: To compare simulated ash clouds produced using Met<sub>P</sub> and Met<sub>70</sub> during the 2019 FSW 18/04 run at T+114 (00:00 23/04/2019) for a plume height of 35 km. (a) Total column mass loading differences, (b) ash cloud area comparison for mass loading values above  $0.2 \text{ g m}^{-2}$ , (c, e, g) flight level layer concentration differences and (d, f, h) ash cloud area comparison for concentrations above  $200 \mu\text{g m}^{-3}$ . Note: All flight level layers are below 30 km, the contour scales differ for the total column mass loading and flight level layer differences plots, and in the area comparison plots the purple region represents an ash cloud area forecast by both met scenarios.



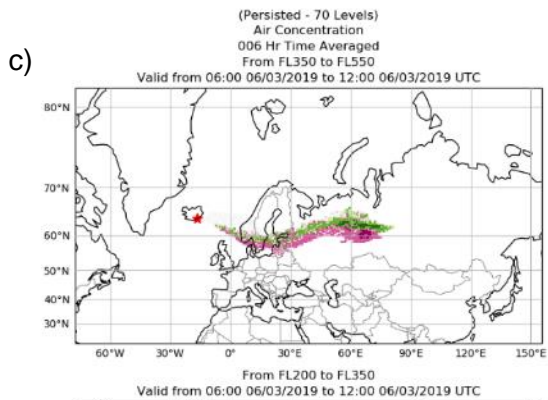
Comparison between 70 Levels of Met and Met Persisted from Level 59



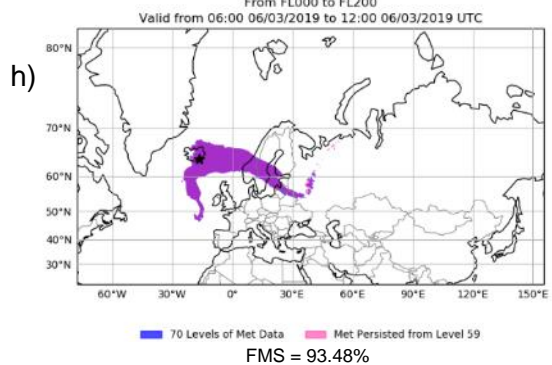
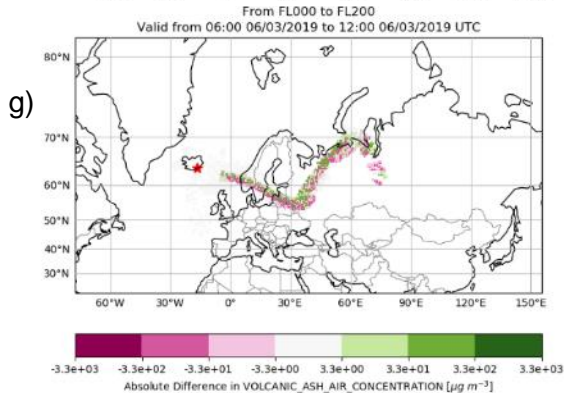
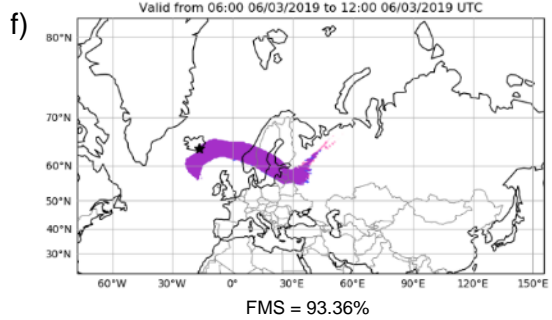
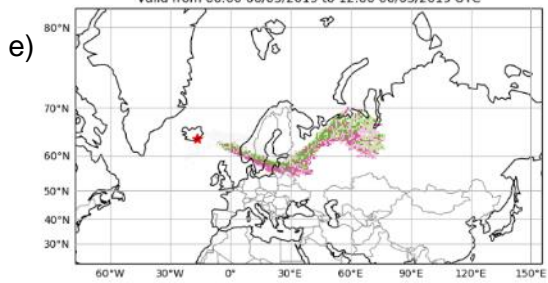
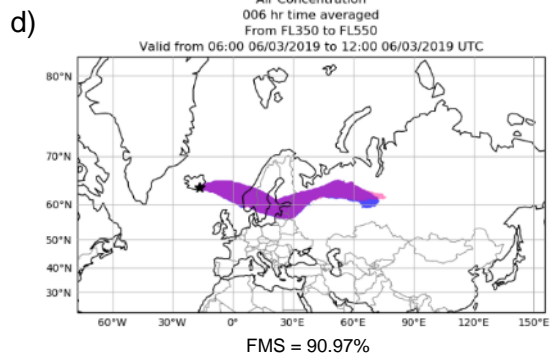
Area Comparison of Regions with  
Volcanic Ash Air Concentrations  $> 0.2\ g\ m^{-2}$



Comparison between 70 Levels of Met and Met Persisted from Level 59

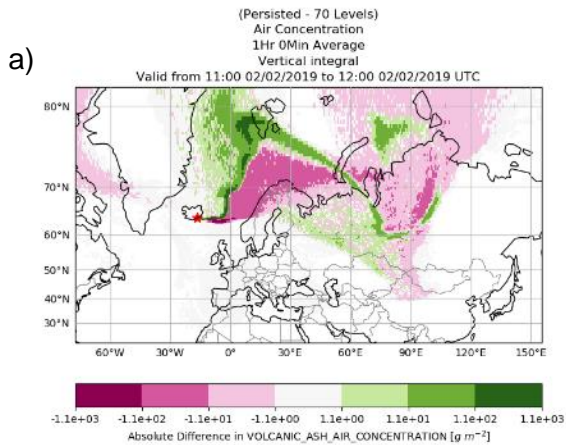


Area Comparison of Regions with  
Volcanic Ash Air Concentrations  $> 200.0\ \mu g\ m^{-3}$

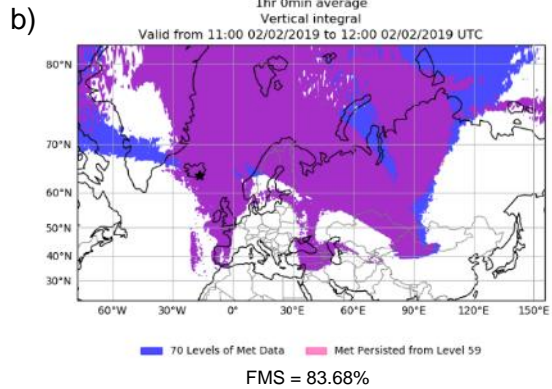


Appendix Figure A8: To compare simulated ash clouds produced using Met<sub>p</sub> and Met<sub>70</sub> during the 2019 VI 04/03 run at T+54 (12:00 06/03/2019) for a plume height of 35 km. (a) Total column mass loading differences, (b) ash cloud area comparison for mass loading values above  $0.2\ g\ m^{-2}$ , (c, e, g) flight level layer concentration differences and (d, f, h) ash cloud area comparison for concentrations above  $200\ \mu g\ m^{-3}$ . Note: All flight level layers are below 30 km, the contour scales differ for the total column mass loading and flight level layer differences plots, and in the area comparison plots the purple region represents an ash cloud area forecast by both met scenarios.

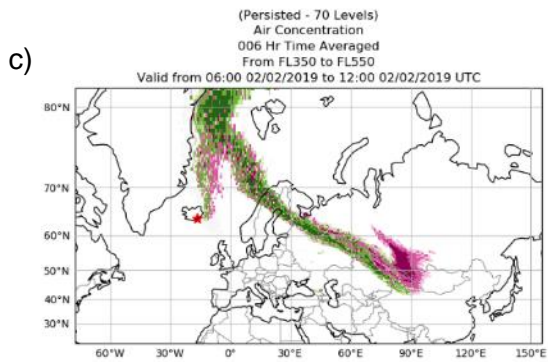
Comparison between 70 Levels of Met and Met Persisted from Level 59



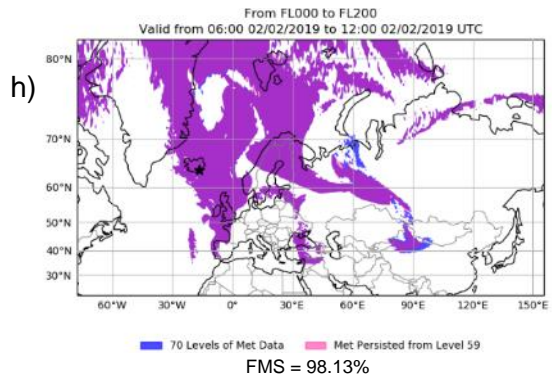
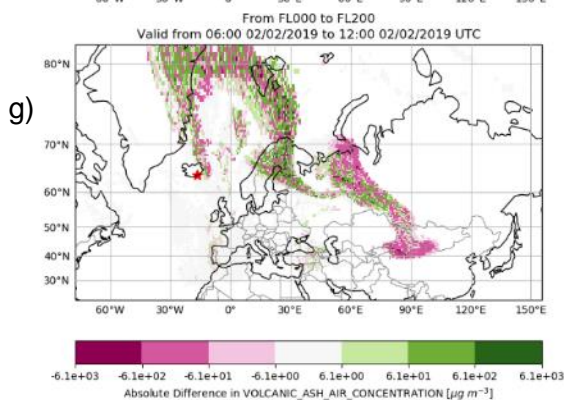
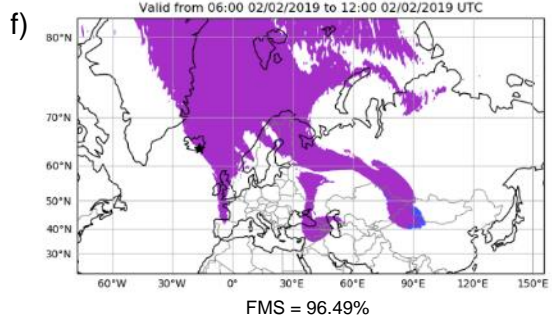
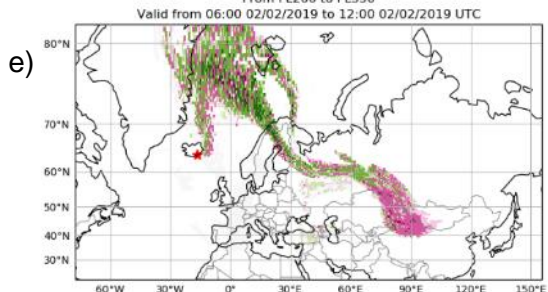
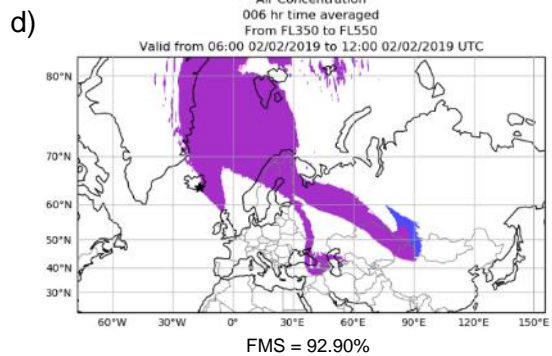
Area Comparison of Regions with  
Volcanic Ash Air Concentrations  $> 0.2\ g\ m^{-2}$



Comparison between 70 Levels of Met and Met Persisted from Level 59



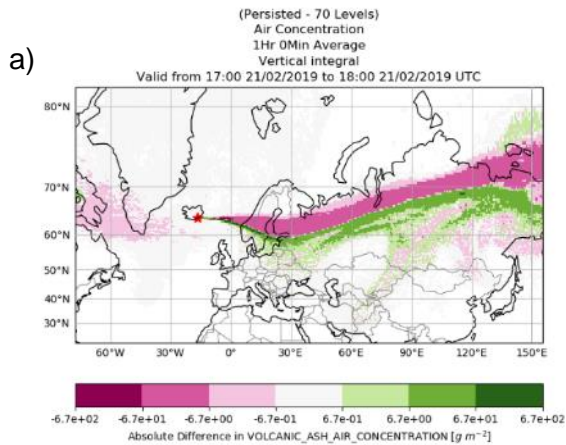
Area Comparison of Regions with  
Volcanic Ash Air Concentrations  $> 200.0\ \mu g\ m^{-3}$



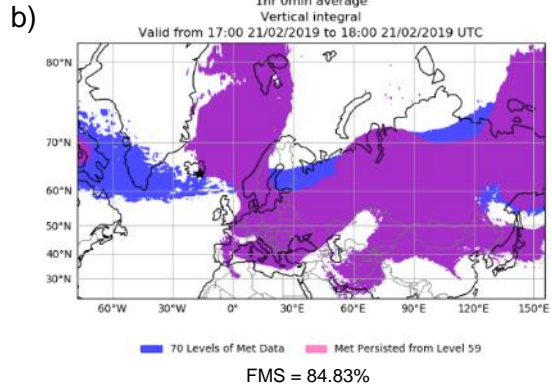
Appendix Figure A9: To compare simulated ash clouds produced using Met<sub>p</sub> and Met<sub>70</sub> during the 2019 VR 28/01 run at T+126 (12:00 02/02/2019) for a plume height of 35 km. (a) Total column mass loading differences, (b) ash cloud area comparison for mass loading values above  $0.2\ g\ m^{-2}$ , (c, e, g) flight level layer concentration differences and (d, f, h) ash cloud area comparison for concentrations above  $200\ \mu g\ m^{-3}$ . Note: All flight level layers are below 30 km, the contour scales differ for the total column mass loading and flight level layer differences plots, and in the area comparison plots the purple region represents an ash cloud area forecast by both met scenarios.



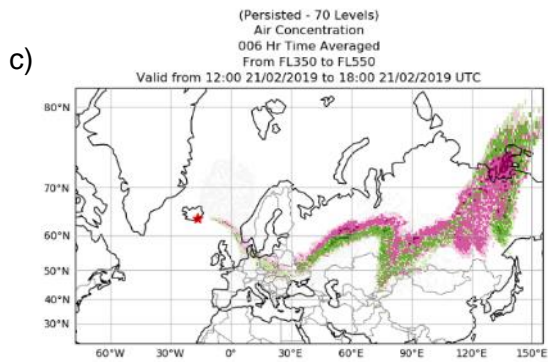
Comparison between 70 Levels of Met and Met Persisted from Level 59



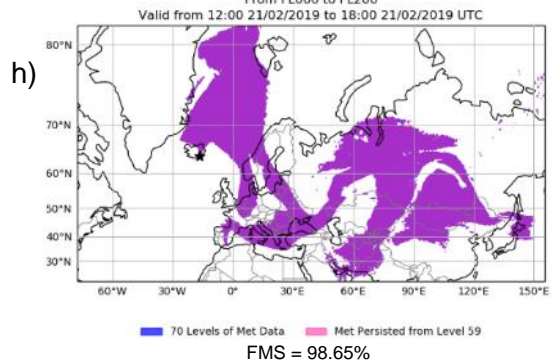
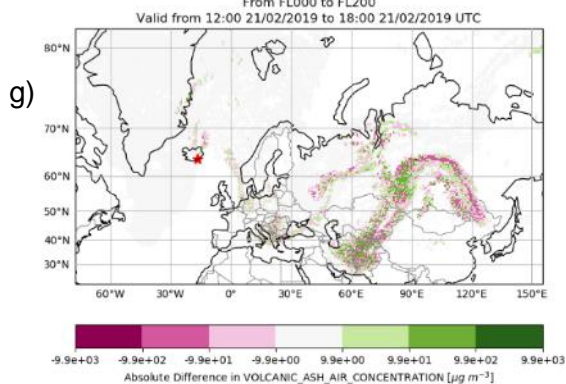
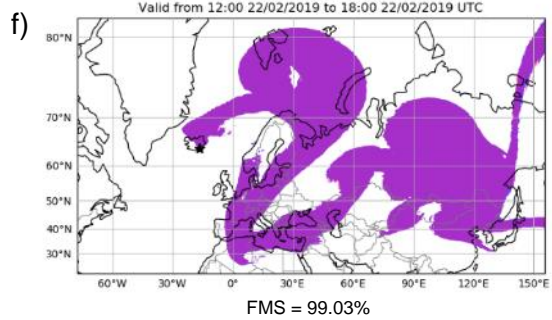
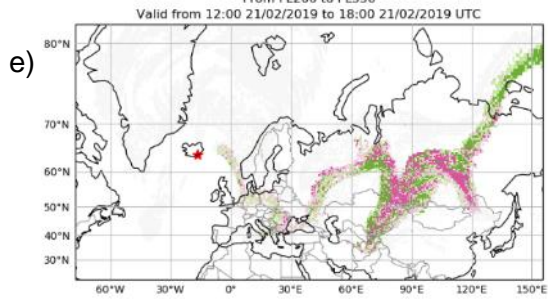
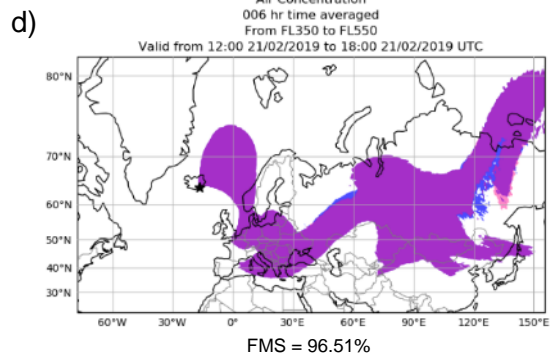
Area Comparison of Regions with  
Volcanic Ash Air Concentrations  $> 0.2\ g\ m^{-2}$



Comparison between 70 Levels of Met and Met Persisted from Level 59



Area Comparison of Regions with  
Volcanic Ash Air Concentrations  $> 200.0\ \mu g\ m^{-3}$



Appendix Figure A10: To compare simulated ash clouds produced using Met<sub>P</sub> and Met<sub>70</sub> during the 2019 VR 16/02 run at T+132 (18:00 21/02/2019) for a plume height of 35 km. (a) Total column mass loading differences, (b) ash cloud area comparison for mass loading values above  $0.2\ g\ m^{-2}$ , (c, e, g) flight level layer concentration differences and (d, f, h) ash cloud area comparison for concentrations above  $200\ \mu g\ m^{-3}$ . Note: All flight level layers are below 30 km, the contour scales differ for the total column mass loading and flight level layer differences plots, and in the area comparison plots the purple region represents an ash cloud area forecast by both met scenarios.

Met Office  
FitzRoy Road  
Exeter  
Devon  
EX1 3PB  
United Kingdom